Thirty-Year Analyses of Seasonal NDVI and Climatic Drivers Across Different Land Cover Types and Biogeographical Regions in Europe

Christina Eisfelder, Soner Üreyen, Sarah Asam, Andreas Hirner, Philipp Reiners, Juliane Huth, Felix Bachofer, Martin Bachmann, Stefanie Holzwarth, and Claudia Kuenzer

Abstract—**Monitoring and analyzing vegetation trends and their climatic drivers are useful to understand the possible impacts of climate change on vegetation. In this study, we analyzed normalized difference vegetation index (NDVI) trends at 1 km^2 resolution for spring (March–May), summer (June–August), and autumn (September–November) for individual biogeographical regions and land cover types in Europe for the 30-year period 1989–2018. In addition, we determined the influence of precipitation, temperature, solar radiation, and vapor pressure deficit (VPD) on the NDVI and identified their influence in areas showing significant ($p<0.05$) negative and positive NDVI trends. Our results show varying seasonal NDVI trends for different regions, ranging between +0.004 and −0.001 NDVI units per year. Highest NDVI increase can be observed for land cover classes in the Pannonian region in autumn (>0.005 NDVI year^{-1}), strongest NDVI decrease (<-0.002 NDVI year^{-1}) for grassland (summer), and rain-fed cropland (autumn) in the Steppic region. In spring, significant positive causal links between the NDVI and temperature are dominant in large areas of Europe while VPD influences the NDVI in north-eastern (positive link) and southern Europe (negative link). In summer, precipitation shows positive causal links to NDVI in parts of the Anatolian and Mediterranean regions, while VPD influences NDVI regionally (negative link). In autumn, precipitation (positive link) and VPD (negative link) are the dominant controlling factors on the NDVI for central-eastern Europe and parts of the Iberian Peninsula. Across Europe, significant positive NDVI trends in spring can be mainly explained by increasing temperatures. Negative spring NDVI trends can be linked to decreasing VPD in some regions. In the Mediterranean, Steppic, and Anatolian regions, a significant NDVI decrease in summer and autumn is mainly linked to decreasing precipitation. The results of this study assist in understanding and quantifying ongoing vegetation change in Europe and reveal the influence climate variables have on the vegetation activity for individual land cover types within different regions.**

Received 20 December 2024; revised 13 February 2025 and 13 March 2025; accepted 23 March 2025. Date of publication 8 April 2025; date of current version 5 May 2025. This work was supported in part by the German Aerospace Center (DLR) TIMELINE Project. *(Corresponding author: Christina Eisfelder.)*

Christina Eisfelder, Soner Üreyen, Sarah Asam, Andreas Hirner, Philipp Reiners, Juliane Huth, Felix Bachofer, Martin Bachmann, and Stefanie Holzwarth are with the German Remote Sensing Data Center (DFD), German Aerospace Center (DLR), 82234 Wessling, Germany (e-mail: christina.eisfelder@dlr.de; soner.uereyen@dlr.de; sarah.asam@dlr.de; andreas.hirner@dlr.de; philipp.reiners@dlr.de; juliane.huth@dlr.de; felix.bachofer@dlr.de; martin.bachmann@dlr.de; stefanie.holzwarth@dlr.de).

Claudia Kuenzer is with the German Remote Sensing Data Center (DFD), German Aerospace Center (DLR), 82234 Wessling, Germany, and also with the Department of Remote Sensing, Institute of Geography and Geology, University of Würzburg, 97074 Würzburg, Germany (e-mail: claudia.kuenzer@dlr.de).

Digital Object Identifier 10.1109/JSTARS.2025.3558816

Index Terms—**Advanced very high resolution radiometer (AVHRR), climate change, driver analysis, Europe, land cover, normalized difference vegetation index (NDVI), vegetation trends.**

I. Introduction

VEGETATION plays an important role in the Earth system [1], [2]. As a key component of the terrestrial ecosystems, it contributes to valuable ecosystem services, such as food production, biodiversity, habitat provision, and water conservation [3], [5], [14] and is an integral part of the global carbon cycle [6], [7], [8]. In recent years, the impacts of climate change on Earth's ecosystems have become more and more evident [9], [10], [11], [12]. Vegetation is particularly influenced by climate as vegetation growth and phenology depend on climate conditions [13], [14], [15]. Europe is the fastest-warming continent, with temperatures rising at around twice the global average rate [16]. Therefore, major impacts on vegetation from climate change are expected, especially in southern regions of Europe [17].

Monitoring past and current vegetation change and trends and their relation to climate variables are useful to understand the possible impacts of climate change on terrestrial ecosystems. Satellite remote sensing has become a standard in monitoring land surfaces as it facilitates spatially continuous and repeatable observation over large areas. Long time periods of at least three decades are required to identify climate-relevant changes and trends [18], [19]. Such area-wide and long time-series on vegetation conditions can be derived from the advanced very high resolution radiometer (AVHRR). AVHRR is the only satellite sensor that provides a time-series of four decades on a daily temporal resolution, going back to the early 1980s. For monitoring the state of vegetation, remote-sensing-based vegetation indices are well established. The most widely used is the normalized difference vegetation index (NDVI), which is calculated as the normalized difference from the spectral reflectance in the near-infrared (NIR) and red spectral domain [20].

Previous studies on long-term vegetation trends have mainly been performed on a global scale with spatial resolutions between 0.5° and 8 km, showing little detail on inner-European variation [21], [22], [23], [24], [25], [26], [27], [28], [29]. Pan-European studies have been conducted by Julien et al. [30], who analyzed NDVI change from the Pathfinder AVHRR Land dataset, and He et al. [31], who derived NDVI trends based on the global inventory modeling and mapping studies NDVI. The previous studies on vegetation trends on a global or European scale report, in general, a greening of vegetation (e.g., [23], [28]).

However, there are regional differences, and for areas in southern and eastern Europe, negative trends were also observed (e.g., [29], [31]).

A novel multidecadal homogeneous NDVI time-series from AVHRR sensors has been generated within the Time-Series Processing of Medium Resolution Earth Observation Data assessing Long-Term Dynamics In our Natural Environment (TIMELINE) project at the German Remote Sensing Data Center (DFD) by the German Aerospace Center (DLR) [19], [32], [33]. The time-series starts in the early 1980s and allows monitoring of climate change-related vegetation dynamics over Europe and North Africa at a 1 km spatial resolution. Although there are other AVHRR time-series products of NDVI such as the National Oceanic and Atmospheric Administration (NOAA) Climate Data Record at 0.05° resolution [34], the TIMELINE-derived information products are the only ones supplied at 1 km over the entire Europe. A previous study by Eisfelder et al. [33] used the TIMELINE NDVI data to derive 30-year NDVI trends for Europe. The study revealed regional patterns and differences among vegetation trends for different seasons. Currently, there is a lack of more detailed analyses on inner-European variation and land-cover-specific trends for individual seasons over Europe. Due to the large variety of ecosystems and their fragmented distribution in Europe, analyses at high spatial resolution including individual land cover classes within different regions of Europe are required.

Moreover, to understand and explain detected NDVI trends, studies usually apply correlation or residual analyses (e.g., [28], [35]). These analyses calculate the relationship between the NDVI and climate variables, including precipitation, temperature, and solar radiation. However, the calculation of the correlation between a set of variables might lead to spurious results and the derived correlation coefficient does not provide any information on the direction of influence between the used variables [36]. In addition, previous studies generally focused on the analysis of the relationship between the NDVI and climate variables at an annual scale (e.g., [37]). However, the climate variables might show different patterns of influences on the NDVI among the different meteorological seasons. In this regard, the use of causal discovery algorithms addresses the aforementioned issues, including the direction of influence as well as minimizing spurious links [36]. Many studies investigating vegetation–climate relationships used, e.g., the Granger causality framework [38], [39]. However, this approach is originally designed for analyzing bivariate relations only. In comparison, the causal discovery algorithm Peter and Clark Momentary Conditional Independence (PCMCI) is designed to evaluate interdependencies of multivariate as well as serially correlated time-series. To this aim, the PCMCI algorithm determines significant causal links between a set of univariate time-series by means of the generation of causal process graphs in consideration of contemporaneous and past temporal lags [36], [40]. Over the last years, PCMCI was frequently applied in the context of vegetation analyses with remote sensing [41], [42], [43]. However, a detailed causal exploration of NDVI drivers at pixellevel and seasonal temporal scale for Europe is lacking so far.

With this study, we aim to close the research gaps regarding more detailed analyses of inner-European NDVI trends on the seasonal scale as well as of NDVI drivers. We investigate the following research questions.

1) What are the seasonal NDVI trends over 30 years within different biogeographical regions in Europe and for individual land cover types?
2) What proportional area of the biogeographical regions and individual land cover types is affected by significant trends of increasing or decreasing vegetation activity?
3) In which areas and for which land cover types are the monthly NDVI time-series driven by meteorological parameters and which parameter shows the largest influence on the NDVI within different seasons?
4) Can seasonal NDVI trends be explained by climate drivers?

II. Study Area

The area covered by this study extends over Europe including continental Europe, Great Britain, and Iceland. The extent toward the North and East is limited by the coverage of the TIMELINE Level 3 NDVI product (see Section III-A). The total area considered amounts to 10 616 503 km^2. The area covers the biogeographical regions in Europe [44] (see Section III-C), as shown in Fig. 1(a). Biogeographical regions present in the northern part of Europe include: Arctic, Boreal, and Alpine. The latter is distributed over mountainous regions throughout the continent. In central Europe, the following regions can be identified from West to East: Atlantic, Continental, Pannonian, and Steppic. Southern Europe is mainly characterized by the Mediterranean biogeographical region, which is complemented by the Black Sea and Anatolian regions in the Southeast. The area proportion of each biogeographical region within the study area is shown in Fig. 1(c). The land cover in Europe is diverse and fragmented. In all biogeographical regions, several land cover types are present. While forest areas dominate northern Europe, a mixture of rain-fed cropland and patches of other land cover types are typical for central and southern Europe.

The analyses performed in this study were limited to areas with stable land cover, i.e., pixels that were assigned the same land cover class in all annual land cover datasets available (see Section III-B). This was done to exclude areas where NDVI trends are influenced by transition to or from other land cover or land uses. The largest areas with stable land cover can be observed for rain-fed agriculture (31% of study area), followed by needleleaf forest (15%), broadleaf forest (11%), grassland (8%), and other forest (8%). The distribution of land cover types in the study area is shown in Fig. 1(b), which presents stable land cover classes derived for this study based on the ESA land cover products [45] (see Section III-B). Fig. 1(d) gives the area proportion for stable pixels of each land cover class within the study area.

III. Data

A. NDVI Monthly Composites

A multidecadal homogeneous NDVI time-series from AVHRR sensors has been generated within the TIMELINE project at the German Remote Sensing Data Center (DFD) by the German Aerospace Center (DLR). The time-series starts in the early 1980s and allows monitoring of global change-related vegetation dynamics over Europe and North Africa at a 1 km spatial resolution [19]. The current TIMELINE products are derived from AVHRR/1, AVHRR/2, and AVHRR/3 data on 12

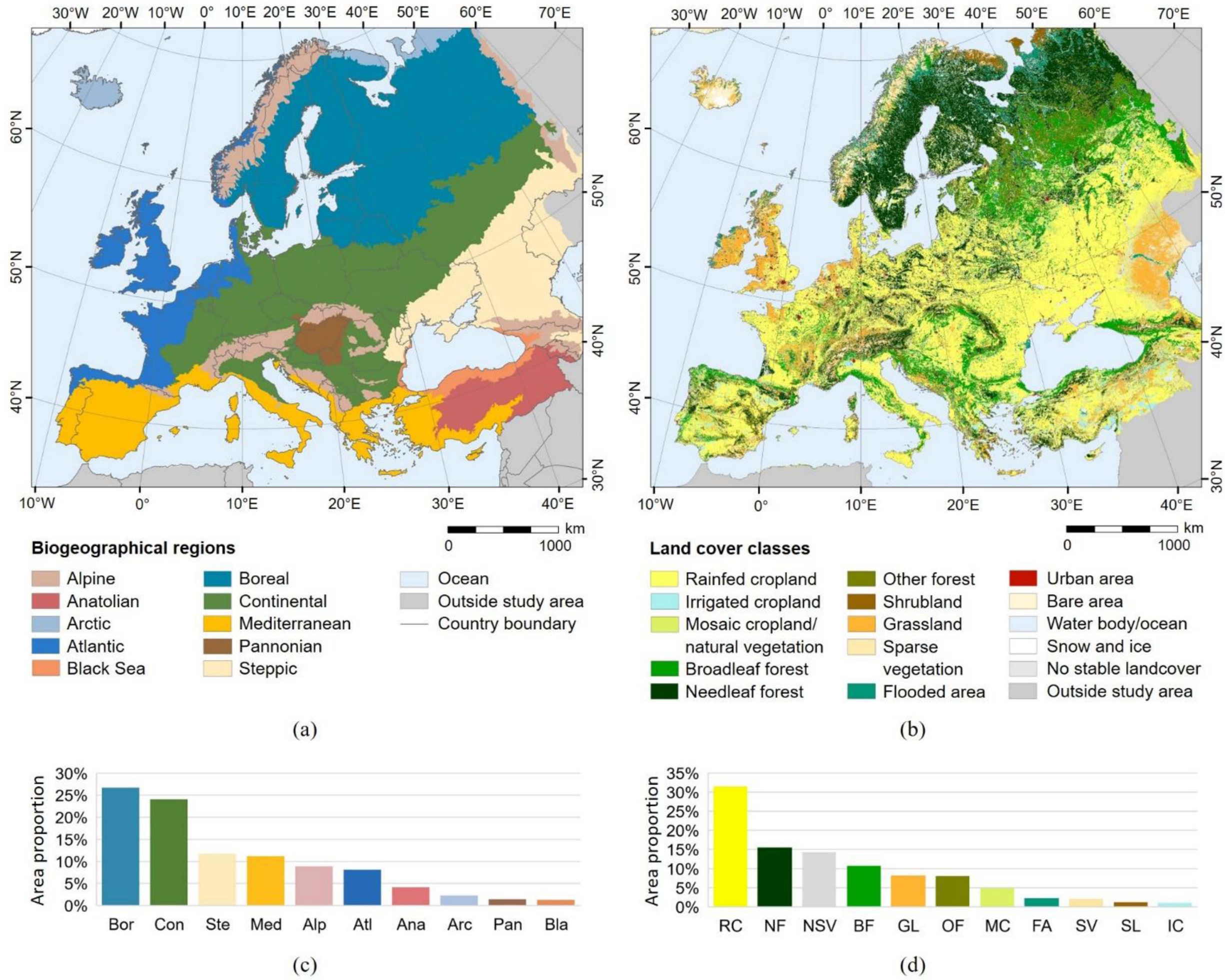

Fig. 1. Study area in Europe with (a) biogeographical regions (as defined by EEA, [44]) and (b) stable land cover (based on the ESA-CCI land cover product [45]). The histograms give (c) area proportion of the biogeographical regions and (d) area proportion of the stable land cover classes within the study area. NSV stands for "no stable vegetation" (includes urban area, bare area, water body, snow and ice, and no stable landcover pixels).

NOAA satellites. A range of preprocessing steps is applied to allow turning the data from different sensors into harmonized analysis-ready data. The preprocessing steps include system correction and calibration, orthorectification, quality flagging, atmospheric correction, and radiometric harmonization [32]. To enable time-series analysis, all data are projected from orbit geometry into a common reference grid in map projection (Lambert Azimuthal Equal Area (LAEA) with ETRS89 datum). The NDVI is finally calculated based on the spectral reflectance measurements in the NIR and red regions using the well-known formula

$$\mathrm{NDVI} = (\mathrm{NIR} - \mathrm{red}) / (\mathrm{NIR} + \mathrm{red}). \tag{1}$$

The TIMELINE Level 3 (L3) NDVI product includes daily, ten-day, and monthly NDVI composites that were created by applying a median compositing approach [32]. The NDVI product is provided in four tiles, covering the extent of the European Environmental Agency (EEA) reference grid, which includes the area from 900 000 m East and 900 000 m North to 7 400 000 m East and 5 500 000 m North [46].

Within this study, the TIMELINE monthly NDVI composites from 1989 to 2018 were used, as for the most northeastern part of the study area, only a few data were recorded in the years before 1989 [33], rendering analyses for these years and regions unreliable. Preprocessing of the data included filling data gaps and smoothing the NDVI time-series on a per-pixel basis, as described in [33]. The applied approach combines "intrayear" interpolation for short gaps with "interyear" interpolation for longer time periods, relies only on the available data of the TIMELINE NDVI product, and maintains the phenological cycle also in case of longer data gaps. A Savitzky–Golay filter was applied in order to remove outliers and to smooth the time-series [33]. This procedure results in a continuous and gap-free NDVI time-series. Finally, the four tiles were mosaicked to retrieve one dataset for each month covering the entire study area.

B. Land Cover Data

The annual ESA climate change initiative (CCI) land cover products provided for the years 1992–2018 with a spatial resolution of 300 m [45] were used to separate among different land cover classes. This product does not cover the first three years of our analysis time-span but it is the only existing

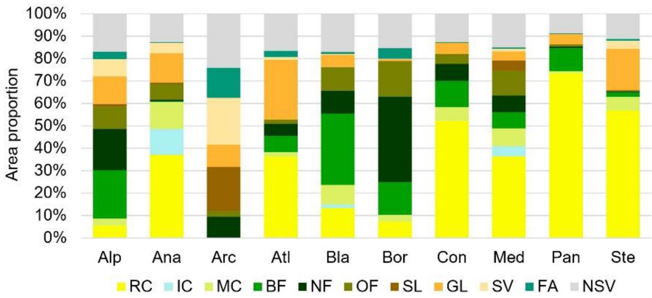

Fig. 2. Area proportion of individual stable vegetation classes within each biogeographical region. The land cover classes are RC: Rain-fed cropland; IC: Irrigated cropland; MC: Mosaic cropland/natural; BF: broadleaf forest; NF: needleleaf forest; OF: other forest; SL: Shrubland; GL: Grassland; SV: Sparse vegetation; FA: Flooded area; NSV: No stable vegetation.

consistent annual LC product going back as far as 1992. The ESA-CCI land cover product differentiates among 37 land cover classes and subclasses. For the current study, these classes were grouped into the following ten vegetation classes and four non-vegetated classes: Rain-fed cropland, Irrigated cropland, Mosaic cropland/natural vegetation, Broadleaf forest, Needleleaf forest, Other forest, Shrubland, Grassland, Sparse vegetation, Flooded area, Urban area, Bare area, Water, Snow, and ice. Table I provides an overview of the land cover classes used within this study and the original CCI classes included. As a second step, the land cover data were resampled to a 1 km spatial resolution in order to match the resolution of the TIMELINE NDVI data by determining the most prevalent land cover class for each pixel. Finally, stable land cover pixels over time were identified. Stable pixels are all pixels that were assigned the same land cover class in all years from 1992 to 2018. The distribution of the stable land cover classes over the study area is shown in Fig. 1(b). The total area covered by all stable vegetated land cover pixels extends to 85.7% of the study area [see Table I, Fig. 1(d)].

C. Biogeographical Regions

The EEA provides a map of biogeographical regions in Europe. This contains the official delineation of regions used in the Habitats Directive. The regions were derived by generalizing natural vegetation maps to describe areas of animal and plant distribution having similar or shared characteristics and similar environmental conditions. The current version used in this study reflects the status of the Biogeographical Regions in Europe from 2016 onwards [44]. The data were downloaded as shapefiles from the EEA Datahub [47]. For inclusion in this study, the polygon data were converted to raster files with 1 km spatial resolution in order to match the NDVI time-series and trend datasets. Fig. 1(a) provides an overview of the spatial extent of the biogeographical regions in the study area. The ten biogeographical regions present in the study area and their area coverage are listed in Table II. Fig. 2 shows the area percentage covered by the above-defined stable vegetated land cover classes for each biogeographical region.

D. ECMWF ERA5-Land Reanalysis Data

Using the ERA5-Land reanalysis data from the European Centre for Medium Range Weather Forecasts (ECMWF) [48], we analyzed the influence of precipitation, temperature, solar radiation, and vapor pressure deficit (VPD) on the NDVI. The ERA5-Land component of the ERA5 reanalysis data comes at an improved spatial resolution of approximately 9 km over the land surface, enabling more detailed spatial analyses compared to the ERA5 data. In particular, we retrieved the variables total precipitation, surface solar radiation downwards, 2-m air temperature, and 2-m dew-point temperature. The reliability of ERA5 precipitation and temperature over Europe was investigated in many studies and the time-series showed good performance (e.g., [49], [50]). In addition, the climate variable VPD was calculated based on the 2-m air temperature and 2-m dew-point temperature using the equation in [51]. VPD proved to be an important driver of vegetation greenness [52], [53], which is why this variable is considered a potential driver of NDVI in this study. Furthermore, the preprocessing of the monthly time-series included the reprojection of the data to the LAEA-ETRS89 (EPSG:3035) coordinate system. In addition, a resampling to 1 km spatial resolution was conducted using the nearest neighbor approach to enable a pixelwise driver analysis of the NDVI.

IV. Methods

A. Seasonal NDVI Trends

The preprocessed TIMELINE NDVI monthly composites were used to derive seasonal trends over the 30-year period 1989–2018. For this, mean NDVI was calculated for spring (March to May), summer (June to August), and autumn (September to November) months. Winter data were excluded from the analysis because the data availability is largely reduced due to insufficient sun illumination. Moreover, large areas in northern Europe are covered by snow in winter, which affects the reflectance signal and thus the NDVI. Mann–Kendall trend test [54], [55] and Theil–Sen Slope Estimator [56], [57] were then performed to identify areas with significant consistent positive or negative trends and to calculate the direction and strength of the trend. The applied method is described in detail in [33]. Significant trends are considered to have p-values lower than 0.05, which is a common threshold representing a statistical significance at the 95% level [23], [26], [58], [59]. The seasonal trends for spring, summer, and autumn were calculated for the four TIMELINE tiles covering the study area and then mosaicked.

For statistical analyses, the areas showing NDVI trends for spring, summer, and autumn intersected with both the preprocessed biogeographical regions (see Section III-C) and stable vegetated land cover (see Section III-B) classes including about 86% of the European land area. These raster data were used to mask areas not of interest, i.e., to regard only specific biogeographical regions and/or land cover classes. In addition, areas with more than 50% missing monthly NDVI composite data and areas with no or little vegetation cover were excluded from the analysis. The NDVI trends for the three seasons were then analyzed with respect to the strength of the trend and with respect to the areas affected by significant/nonsignificant positive or negative trends for all combinations of individual biogeographical regions and vegetated land cover classes.

B. NDVI Driver Analysis

The PCMCI$^+$ algorithm was used to determine the influence of the climate variables precipitation, temperature, solar

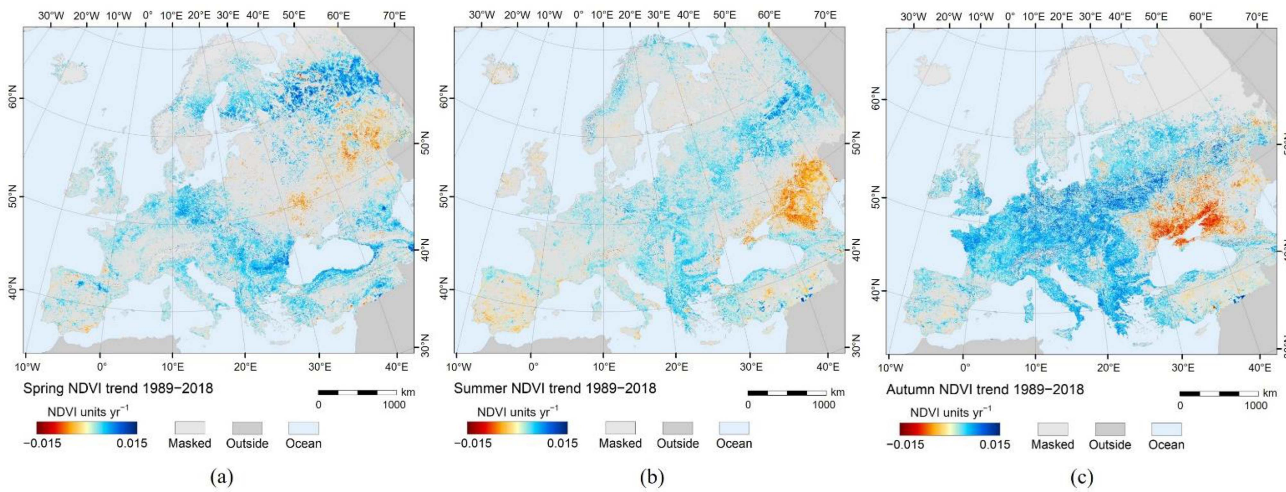

Fig. 3. NDVI trend for (a) spring, (b) summer, and (c) autumn for the period 1989–2018 derived from the TIMELINE level 3 monthly NDVI time-series [33] for the study area in Europe. The masked area includes insignificant trends ($p \geq 0.05$), pixels with no or little vegetation cover (mean annual NDVI <0.2), and areas with more than 50% missing monthly NDVI composites.

radiation, and VPD on the monthly NDVI [60]. PCMCI$^+$ enables the determination of contemporaneous (lag 0) and lagged causal links for the investigated time-series. In contrast to the standard PCMCI, PCMCI$^+$ is capable of detecting the causal direction of contemporaneous links. In general, PCMCI consists of two main steps to determine significant causal links. The first step retrieves potential time lagged drivers, also called causal parents, for each used variable by means of a version of the Peter and Clark (PC) algorithm. This step runs iteratively on each variable using the partial correlation as an independence test. The result of this step is a set of causal parents for each investigated variable. However, at this stage, the potential causal parents might include false positives. For this purpose, the second step covers the momentary conditional independence (MCI) test to extract the significant causal links given the identified sets of causal parents of the considered variables from the first PC step. Ultimately, the causal parents that pass the MCI test will be considered as causal links [36], [40].

In this study, the used time-series had a monthly temporal resolution and the entire analysis was conducted at 1 km pixel level. To evaluate the temporal dependencies of the climate variables on the monthly NDVI, a temporal lag of three months was allowed. Considering the temporal lags, the observations of the drivers were allowed to be outside of the considered season. Next, a causal link was considered significant if the p-value was lower than 0.1. Furthermore, the time-series were preprocessed prior to the application of the PCMCI algorithm to meet several assumptions of this approach [61]. First, we removed the linear trend of the time-series using the least square fit and then calculated seasonal anomalies to meet the stationarity requirement when using the partial correlation as an independence test. The seasonal anomalies were calculated by subtracting the respective observations from the long-term seasonal average. Next, to meet the causal stationarity assumption, we performed the driver analysis at seasonal temporal scale for the seasons spring, summer, and autumn. Here, the temporal lags of the time-series include observations prior to the investigated season as well. In addition, certain NDVI pixels were excluded from the driver analysis. For this, the same rules were applied as for the trend analysis (see Section IV-A).

In a further step, the results from the driver analysis were used to identify the climate influence on the NDVI for individual land cover types within each of the biogeographical regions for the three seasons. Therefore, for each land cover type within each region, the average MCI, giving the strength of the influence resulting from the NDVI driver analysis, was calculated.

For identifying possible drivers of observed NDVI trends, we analyzed the influence of meteorological variables within areas showing significant positive or negative NDVI trends only. Therefore, the MCI dataset was overlayed with the NDVI trends and filtered for areas with significant positive or negative NDVI trends. The average MCI was then derived separately for the individual stable land cover classes within each biogeographical region and for the three seasons.

V. Results

A. Regional and Land Cover-Specific Seasonal NDVI Trends

The seasonal NDVI trends are shown in Fig. 3. A mask was applied to show only significant ($p<0.05$) trends. The masked area also includes pixels with no or little vegetation cover characterized by a mean annual NDVI of less than 0.2 (e.g., [62], [63], [64], [65]) and areas with more than 50% missing monthly NDVI composite data within the respective season in the period 1989–2018. Missing data occur due to persistent cloud cover, especially in autumn over northern Europe due to insufficient sun illumination [33]. The area affected by significant positive trends ranges between 21% (spring) and 25% (autumn) of the entire study area. Significant negative trends occur for 4% to 6% of the land area.

The diagrams in Fig. 4 show the mean NDVI trends over individual biogeographical regions for spring, summer, and autumn. Although the regionally averaged trends are overall low because all positive and negative values are included in

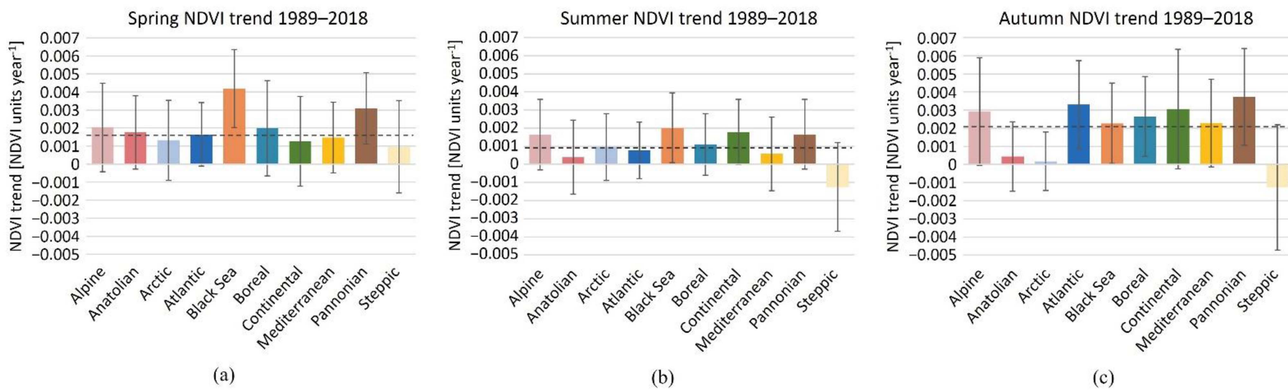

Fig. 4. Mean NDVI trend for each biogeographical region for the three seasons of (a) spring, (b) summer, and (c) autumn within the period 1989–2018. The vertical lines give the standard deviations, and the dashed horizontal lines give the average trend for each season for the entire study area in Europe.

the average, they allow for a general comparison among seasons and regions. In spring [see Fig. 4(a)], the average NDVI trend for the study area in Europe is positive with 0.0016 NDVI units per year (dashed line). Two regions show exceptionally high positive NDVI trends. These are the Black Sea and Pannonian regions. Lower than average are the trends within the Mediterranean, Arctic, Continental, and Steppic regions.

In summer [see Fig. 4(b)], most regions show very low positive NDVI trends with an average of about 0.001 NDVI units per year. Highest positive trends can be observed for the Black Sea, Continental, Pannonian, and Alpine regions. The Steppic region is the only region with an overall negative summer NDVI trend.

The average NDVI trend over the study area is strongest positive in autumn [see Fig. 4(c)] with 0.0021 NDVI units per year. Two different groups of regions can be observed in this season. On the one hand, seven of the ten regions experience NDVI trends higher than this average, with the highest values observed for the Pannonian, Atlantic, and Continental regions. On the other hand, there are two regions (Anatolian and Arctic) with almost no trend and one region (Steppic) for which a negative NDVI trend can be detected in autumn.

The trends for the different biogeographical regions indicate that regions in western and central Europe (Atlantic, Continental, Mediterranean, and Pannonian) tend to show a stronger positive NDVI trend in autumn compared to spring and summer. In contrast, the regions toward the South-East (Steppic, Black Sea, and Anatolian) have a stronger positive NDVI trend in spring and lower positive or negative NDVI trends in summer and autumn.

The analysis of the seasonal NDVI trends for individual land cover classes can further provide information about differences among land cover types. Fig. 5 gives the mean seasonal NDVI trends for spring, summer, and autumn for the individual land cover types within each biogeographical region. The NDVI trends are given in NDVI units per year. As an example, a trend of 0.004 NDVI units per year corresponds to an NDVI increase of 0.12 NDVI units over the 30-year period of investigation.

Fig. 5 reveals that individual land cover classes show highly different seasonal NDVI trends among regions. Also, land cover classes within one region can differ largely. For the Black Sea region in spring [see Fig. 5(a)], for example, we find that the comparatively high NDVI increase results mainly from an increase of four land cover classes. These are rain-fed cropland, mosaic cropland/natural, broadleaf forest, and needleleaf forest. The other land cover classes do not show outstanding high NDVI trends. For the Pannonian region, in contrast, similarly high positive NDVI trends can be observed across all land cover classes in spring, except for irrigated cropland [see Fig. 5(a)]. In summer, the differences in the Pannonian region are larger. Here, the three forest classes show higher positive NDVI trends compared to other land cover classes in this region [see Fig. 5(b)].

In autumn, all land cover classes in the Pannonian region experience strong NDVI increase [see Fig. 5(c)], with the highest values for mosaic cropland/natural, the three forest classes, flooded area, and grassland. In the Continental region, also several classes contribute to the overall positive autumn NDVI trend. In the Atlantic region, rain-fed cropland and mosaic cropland/natural show higher positive NDVI trends compared to other land cover classes in autumn. Especially rain-fed cropland, but also grassland, due to their large area coverage (compare Fig. 2), contribute to the positive autumn NDVI trend in this region.

B. Area With Negative or Positive NDVI Trends

For each biogeographical region and each land cover class, we additionally derived the percentage of stable land cover pixels, which show a negative or positive seasonal NDVI trend within the period 1989–2018. The diagrams in the upper row in Fig. 6(a)–(c) give the results for the three seasons of spring, summer, and autumn for biogeographical regions. Different intensities of color differentiate between significant ($p < 0.05$) and nonsignificant ($p \geq 0.05$) trends. Areas with nonsignificant trends are included in the figures in order to provide information about the tendency of trends for the entire study area coverage. The diagrams in the lower row show percentual areas affected for individual land cover classes [see Fig. 6(d)–(f)].

In spring, the two regions with the highest average positive NDVI trend (compare Fig. 4), Pannonian and Black Sea, also show outstanding high percentages of the area with a significant positive trend [see Fig. 6(a)]. The other regions have significant positive trends in about 20% –30% of their area, while negative trends are mostly not significant in spring. Larger areas (>10%) with significant negative NDVI trends can be observed in summer [see Fig. 6(b)] in the Mediterranean and Anatolian

Spring NDVI trend

	Alp	Ana	Arc	Atl	Bla	Bor	Con	Med	Pan	Ste
RC	0.0021	0.0019	N/A	0.0019	0.0048	0.0000	0.0009	0.0016	0.0030	0.0008
IC	0.0009	0.0018	N/A	0.0002	0.0029	N/A	0.0008	0.0015	0.0014	0.0022
MC	0.0017	0.0017	N/A	0.0017	0.0045	0.0005	0.0010	0.0017	0.0036	0.0008
BF	0.0022	0.0022	-0.0003	0.0014	0.0043	0.0032	0.0018	0.0019	0.0032	0.0016
NF	0.0019	0.0028	0.0003	0.0017	0.0044	0.0019	0.0023	0.0014	0.0033	0.0011
OF	0.0025	0.0017	0.0011	0.0012	0.0033	0.0028	0.0020	0.0011	0.0034	0.0010
SL	0.0014	0.0010	0.0016	0.0010	N/A	0.0027	0.0033	0.0013	N/A	0.0017
GL	0.0013	0.0014	0.0009	0.0016	0.0026	0.0002	0.0014	0.0016	0.0035	0.0012
SV	0.0005	0.0014	0.0003	0.0012	0.0015	0.0020	0.0003	0.0007	N/A	0.0009
FA	0.0026	-0.0011	0.0009	0.0010	0.0021	0.0015	0.0006	0.0007	0.0031	0.0019

(a)

Summer NDVI trend

	Alp	Ana	Arc	Atl	Bla	Bor	Con	Med	Pan	Ste
RC	0.0018	-0.0001	N/A	0.0008	0.0016	0.0016	0.0014	0.0002	0.0013	-0.0010
IC	0.0016	0.0014	N/A	-0.0002	0.0014	N/A	0.0024	0.0009	0.0006	0.0026
MC	0.0020	0.0004	N/A	0.0013	0.0027	0.0031	0.0027	0.0003	0.0028	-0.0012
BF	0.0020	0.0013	0.0008	0.0016	0.0018	0.0018	0.0024	0.0019	0.0034	0.0016
NF	0.0014	0.0015	0.0011	0.0006	0.0022	0.0005	0.0024	0.0011	0.0032	0.0006
OF	0.0019	0.0008	0.0013	0.0011	0.0022	0.0010	0.0022	0.0005	0.0036	0.0005
SL	0.0021	0.0004	0.0017	-0.0004	N/A	0.0018	0.0033	0.0008	N/A	-0.0004
GL	0.0010	0.0003	0.0008	0.0004	0.0022	0.0007	0.0013	0.0002	0.0020	-0.0023
SV	0.0016	0.0004	0.0011	0.0005	0.0007	0.0013	-0.0002	0.0003	N/A	-0.0016
FA	0.0010	-0.0019	0.0012	-0.0003	0.0024	0.0005	0.0019	-0.0001	0.0027	0.0006

(b)

Autumn NDVI trend

	Alp	Ana	Arc	Atl	Bla	Bor	Con	Med	Pan	Ste
RC	0.0027	0.0001	N/A	0.0037	0.0018	0.0024	0.0023	0.0021	0.0032	-0.0021
IC	0.0010	0.0013	N/A	0.0004	0.0008	N/A	0.0021	0.0011	0.0045	0.0036
MC	0.0020	0.0005	N/A	0.0032	0.0024	0.0030	0.0034	0.0021	0.0058	0.0003
BF	0.0024	0.0012	-0.0002	0.0026	0.0025	0.0018	0.0035	0.0035	0.0056	0.0011
NF	0.0028	0.0017	0.0003	0.0025	0.0029	0.0015	0.0042	0.0028	0.0054	0.0007
OF	0.0031	0.0007	0.0003	0.0028	0.0023	0.0014	0.0040	0.0021	0.0054	0.0015
SL	0.0005	0.0008	0.0004	-0.0008	N/A	0.0005	0.0048	0.0031	N/A	0.0008
GL	0.0018	-0.0002	-0.0004	0.0029	0.0012	0.0026	0.0039	0.0020	0.0050	-0.0002
SV	0.0010	0.0005	-0.0003	0.0016	0.0002	0.0007	0.0023	0.0009	N/A	-0.0007
FA	0.0011	-0.0008	0.0008	0.0021	0.0029	0.0018	0.0040	0.0014	0.0054	0.0013

(c)

Fig. 5. Mean NDVI trend for individual land cover classes within the biogeographical regions for (a) spring, (b) summer, and (c) autumn for the period 1989–2018.

regions, and, most prominent, in the Steppic region, where 27% of the area have a significant decreasing summer NDVI. The Steppic region is the only region with larger areas affected by negative trends than by positive trends, both in summer and autumn. Except for the Steppic, Arctic, and Anatolian regions, all other regions feature significant positive trends for at least 45% of their area in autumn.

Comparing the area affected by significant NDVI trends for individual land cover classes, we find similar patterns for all classes in spring [see Fig. 6(d)]. In summer and autumn, differences among land cover classes are larger. Broadleaf forest shows the largest area with significant positive trends (49%) in summer and almost no area with significant negative trends, while the classes grassland and sparse vegetation have similar percentage areas (about 17%) with significant negative and significant positive trends. In autumn, sparse vegetation and rain-fed cropland show the largest percentage area with significant negative NDVI trends (12% –13%) [see Fig. 6(f)]. Sparse vegetation also has the smallest area with significant positive trends from all land cover classes in autumn. The other classes show a maximum area with significant positive trends (30% –63%) in autumn, with the largest areas observed for the three forest classes. For all three seasons, the largest percentage area with significant positive trends can be observed for the broadleaf forest.

In Fig. 11, a series of diagrams is provided that give the percentual area for individual stable land cover classes with negative or positive trends for each biogeographical region. Fig. 7 includes the diagrams for the four largest biogeographical regions. In the Continental region [see Fig. 7(a)], the percentage area with significant positive NDVI trends becomes larger from spring to summer to autumn for most land cover classes. In autumn more than 42% of the area for all classes has significant positive NDVI trends. For some land cover classes (sparse vegetation, cropland classes), small percentual areas with significant negative trends can also be observed in spring. Only sparse vegetation shows significant negative trends for more than 20% of its area in summer. For the Mediterranean region [see Fig. 7(b)], a higher percentage of area with negative trends can be observed in summer for all land cover classes compared to spring and autumn. Areas with significant negative trends reach between 4% and 19% in summer. However, significant positive trends are

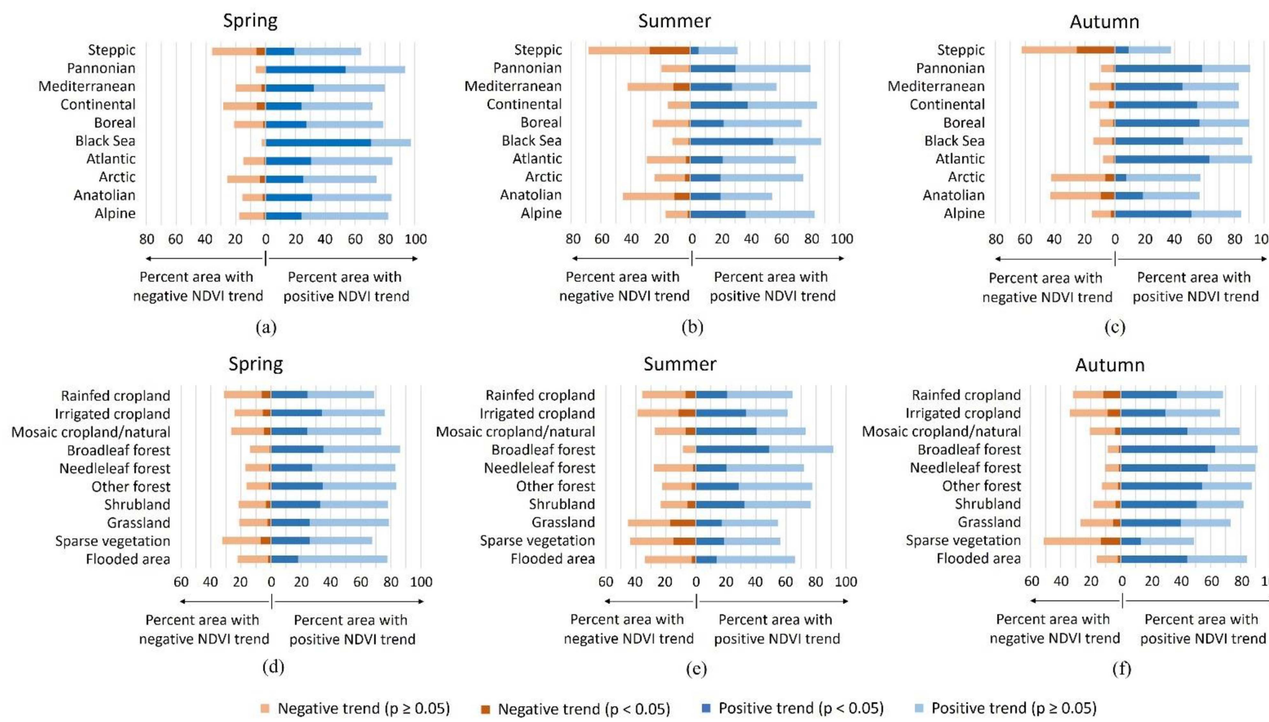

Fig. 6. Percent area with negative (red) or positive (blue) NDVI trends within each biogeographical region for (a) spring, (b) summer, and (c) autumn. Percent area with negative or positive NDVI trends for individual land cover classes for (d) spring, (e) summer, and (f) autumn. Different intensities of color differentiate between significant ($p<0.05$, dark red and blue) and nonsignificant ($p\geq0.05$, bright red and blue) trends.

present at larger areas of between 18% for rain-fed cropland and 59% for broadleaf forest. In the Boreal region [see Fig. 7(c)], we observe varying percentages of area among land cover classes with negative or positive NDVI trends. The area with significant positive trends ranges from <9% for grassland and cropland to 27% for needleleaf forest and >40% for broadleaf and other forest in spring. In summer, needleleaf forest and other forest show comparatively small areas with significant positive trends. In autumn all land cover classes in the Boreal region have significant positive NDVI trends for between 1/3 and 2/3 of their area. In the Steppic region [see Fig. 7(d)], trends differ largely among land cover classes, especially in summer and autumn. In spring, all classes show significant positive NDVI trends for 12% –26% (except for irrigated cropland) and significant negative trends for <8% of the area. In summer, especially grassland and sparse vegetation show large areas with decreasing vegetation activity. About 53% of the area is covered by grassland and 40% of sparse vegetation, as well as 25% of mosaic cropland/natural, and 19% of rain-fed cropland show significant negative NDVI trends in this region in summer. In autumn, the trends are similar to summer, but the area with significant negative trends decreased for several classes, especially for grassland and sparse vegetation. However, rain-fed cropland shows with 36% an even larger area percentage with significant negative NDVI trends in autumn.

C. Seasonal NDVI Drivers

Fig. 8 shows the relationships, the strength of the influence, and temporal lags between the climatic variables precipitation, temperature, solar radiation, and VPD with the NDVI per season during 1989–2018. Separate figures for all variables showing their strength of influence and temporal lags can be found in Figs. 12 and 13, respectively. In addition, Fig. 14 provides bar charts showing the strength of influence of the climate variables on the NDVI for the individual land cover classes within each of the biogeographical regions for the three seasons.

In spring, significant causal links between the NDVI and temperature are dominant in large areas of Europe, with strongest influences observed in the Black Sea, Continental, Pannonian, Alpine, and Steppic regions, as well as for South-West Boreal (see Figs. 8(a), 12(d), and 14). As demonstrated in Fig. 8(d), this coupling between temperature and the NDVI is positive and indicates that vegetation growth over these regions is controlled by temperature. The positive influence of temperature on the NDVI is present for almost all classes in all regions, with forest classes often most influenced (see Fig. 14). Also, it was found that the NDVI response to temperature takes place with a temporal lag of 1 month [see Figs. 8(g) and 13(d)]. Besides temperature, VPD was found to influence the spring NDVI, especially in parts of the Anatolian, Boreal, Mediterranean, and Steppic regions [see Figs. 8(a) and 12(j)]. This coupling between the VPD and the NDVI was found to be negative in southern parts (Anatolian, Black Sea, Mediterranean, and Steppic) and positive in northern and mountainous regions (Arctic, Boreal, and Alpine) of Europe (see Figs. 12(j) and 14). In spring, precipitation and solar radiation appear to control the NDVI only regionally in parts of the Anatolian, Mediterranean, and Steppic biogeographical regions [see Fig. 12(a) and (g)].

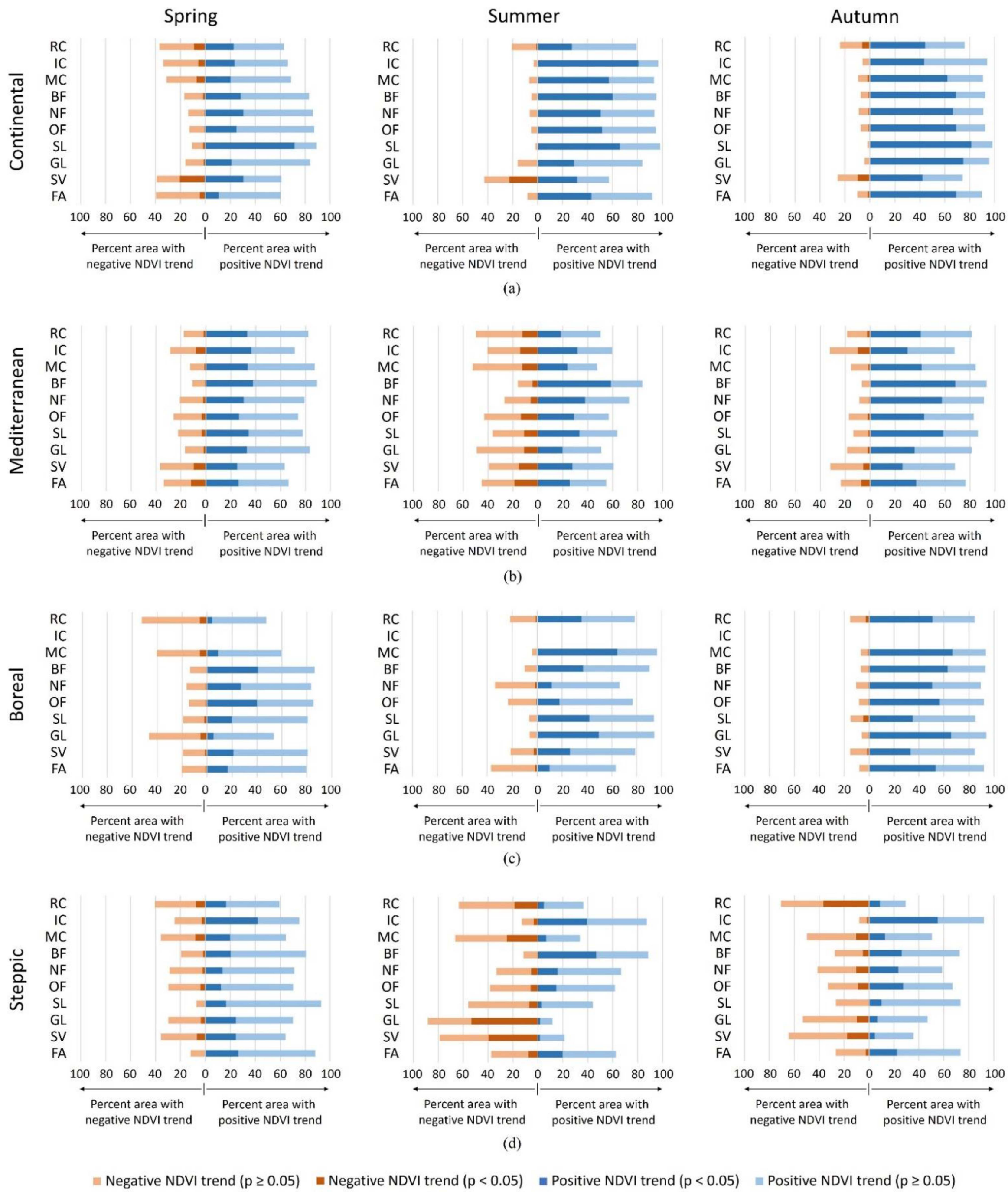

Fig. 7. Percent area with negative (red) or positive (blue) NDVI trends for individual land cover classes within the biogeographical regions (a) Continental, (b) Mediterranean, (c) Boreal, and (d) Steppic for spring (left), summer (center), and autumn (right). Different intensities of color differentiate between significant ($p<0.05$, dark red and blue) and nonsignificant ($p\geq0.05$, bright red and blue) trends. The land cover classes are RC: Rain-fed cropland; IC: Irrigated cropland; MC: Mosaic cropland/natural; BF: broadleaf forest; NF: Needleleaf forest; OF: Other forest; SL: Shrubland; GL: Grassland; SV: Sparse vegetation; FA: Flooded area.

In summer, precipitation was found to have a positive influence on the NDVI in parts of the Anatolian and Mediterranean regions [see Fig. 8(b) and (e)], especially affecting the land cover classes grassland, rain-fed cropland, mosaic cropland/natural, and sparse vegetation (see Fig. 14). This coupling is particularly pronounced in parts of Spain and Türkiye [see Fig. 12(b)]. For most of the pixels, the temporal lag was found to be at one month [see Fig. 13(b)]. Regions where the NDVI was influenced by temperature shifted north as compared to spring. In detail, a positive coupling between temperature and the NDVI was found in Northern Scandinavia, including the regions Alpine, Arctic, and Boreal [see Fig. 12(e)]. Solar radiation indicated a negative coupling with the NDVI in the Mediterranean, particularly on the Iberian Peninsula [see Figs. 8(b), (e), and 12(h)]. The variable

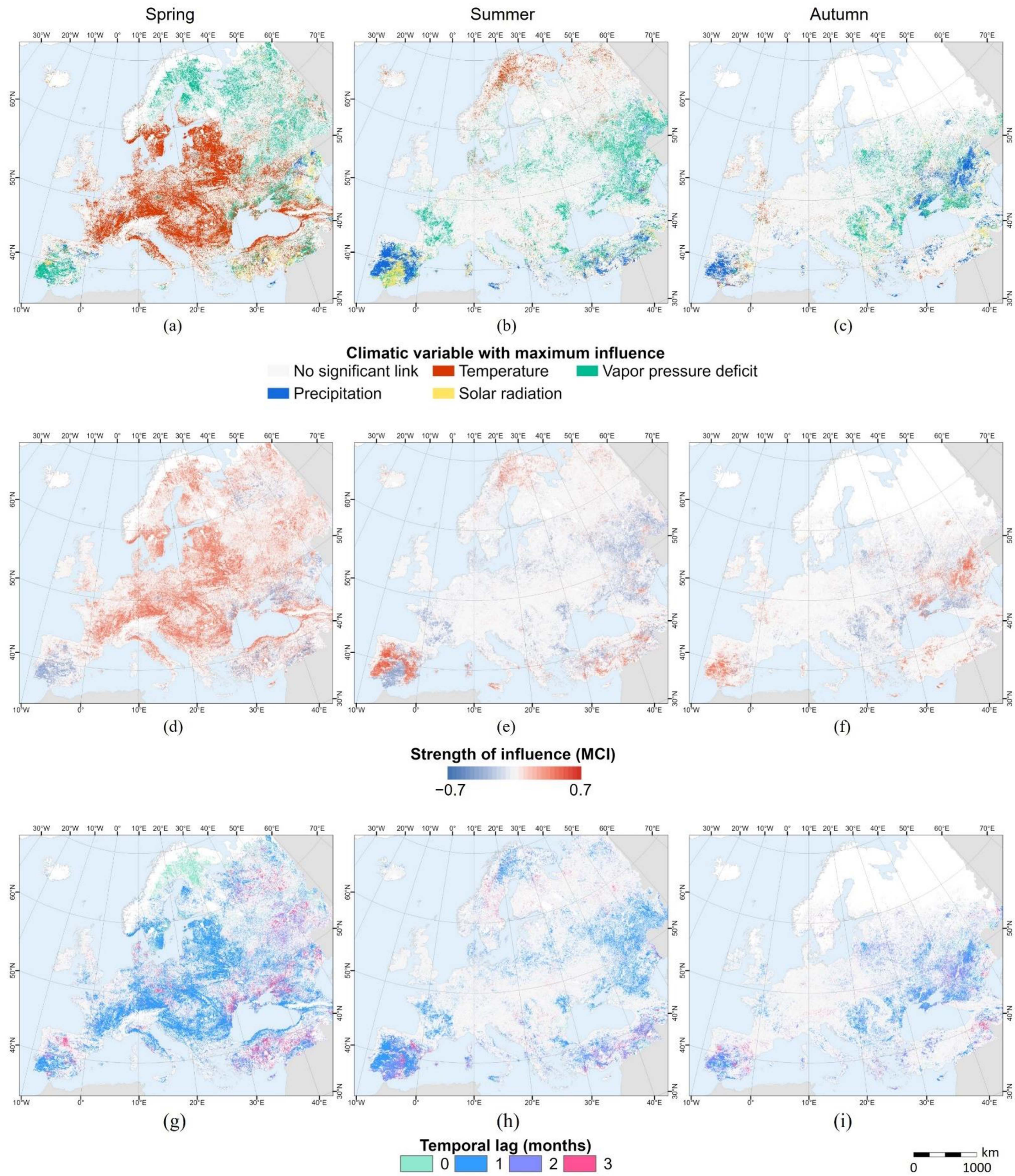

Fig. 8. Climate drivers having the largest influence on the (a)–(c) NDVI per season as well as the (d)–(f) strength of their influence and (g)–(i) their temporal lag, respectively. The strength of the influence is measured by the MCI test, which is the partial correlation coefficient. Pixels in light gray color have no causal link. Pixels in white were excluded from the analysis due to a low NDVI value or data availability.

VPD was found to influence the NDVI regionally in many biogeographic regions, including parts of the Anatolian, Atlantic, Boreal, Mediterranean, and Steppic regions [see Figs. 8(b) and 12(k)]. This coupling is negative and dominant at a temporal lag of 1 month [see Fig. 13(k)]. Land cover classes most strongly influenced by VPD in summer include grassland, mosaic agriculture/natural, shrubland, and sparse vegetation, especially in the Steppic and Anatolian regions, as well as grassland in the Pannonian region. Forest classes are less affected by VPD (see Fig. 14). For large parts of the Continental biogeographic region, no significant causal links were identified in summer [see Fig. 8(b)].

The variables precipitation and VPD appear to be the dominant controlling factors on the NDVI in autumn [see Fig. 8(c)]. For example, the influence of precipitation on the NDVI in the Southern Iberian Peninsula remained positive in autumn [see Fig. 12(c)]. In addition, precipitation had a positive influence on the NDVI in the Steppic region [see Fig. 12(c)]. These positive couplings between the NDVI and precipitation were mostly characterized by a temporal lag of one month [see Fig. 13(c)]. In both regions, especially grassland, mosaic cropland/natural and rain-fed agriculture showed to be influenced by precipitation (see Fig. 14). On the other hand, the NDVI showed a negative response to VPD in Eastern parts of Europe, including the regions Boreal, Continental, Pannonian, and Steppic [see Fig. 12(l)]. The dominant temporal lag for this coupling was at one month as well [see Fig. 13(l)]. The variables temperature and solar radiation were found to have less influence on the NDVI in terms of their spatial occurrence [see Fig. 12(f) and (i)]. For example, temperature showed positive influences on the NDVI in small parts of the Atlantic and Mediterranean regions.

D. Climate Drivers of Significant NDVI Trends

Fig. 9 shows the strength of the influence of the meteorological variables (temperature, precipitation, solar radiation, and VPD) in areas with significant NDVI trends in the period 1989–2018. The diagrams for each biogeographical region separate between significant negative and significant positive NDVI trends and give the relation for each of the three seasons (spring, summer, and autumn). The strength of influence is presented for the four land cover classes with the largest area coverage in the study area (rain-fed cropland, broadleaf forest, needleleaf forest, and grassland), covering together two-third of the study area in Europe (see Table I).

Fig. 9 reveals that in several regions, positive NDVI trends in spring are influenced by increasing temperatures (red bars in all graphs). This is especially the case in the Continental, Pannonian, Steppic, Black Sea, Anatolian, and Alpine biogeographical regions. In five of these six regions, the strength of the influence is the strongest between temperature and broadleaf forest. In some regions, including the Steppic and Anatolian regions, also a relation to decreasing VPD can be observed for areas with increasing NDVI with the strongest influence for rain-fed cropland. For summer and autumn, the areas with positive NDVI trends do not show pronounced influence from the meteorological variables (see Fig. 9). A slight negative coupling to VPD can be observed in some regions. Positive trends for rain-fed cropland and grassland in the Anatolian are positively linked to precipitation in summer, and increased grassland NDVI in the Pannonian shows to be influenced by solar radiation in autumn.

Areas with negative NDVI trends in spring show considerable influence from VPD in the Continental, Boreal, Steppic, Anatolian, and Alpine regions (see Fig. 9). In the Pannonian region, areas of rain-fed cropland and grassland with decreasing NDVI experienced decreasing temperatures (positive coupling). In the Mediterranean region, a strong influence of the meteorological variables on areas with negative NDVI trends can be observed in summer. Decreasing NDVI is most influenced by decreasing precipitation (positive coupling) but also by increasing solar radiation (negative coupling), especially for broadleaf forest, grassland, and rain-fed cropland. Similar but weaker relations can be observed in autumn in the Mediterranean region. A negative coupling to VPD can also be found for areas with negative NDVI trends in summer and autumn in the Boreal, Steppic, and Anatolian regions. In the Anatolian region, however, negative trends in summer are strongly influenced by decreasing precipitation. Similar to the Mediterranean, negative NDVI trends in autumn also show mainly a positive coupling to decreasing precipitation in the Steppic region (see Fig. 9).

VI. Discussion

A. Significance of Seasonal NDVI Trend Analyses at 1 Km Resolution Over Europe

In this study, we present analyses of seasonal NDVI trends for biogeographical regions and individual land cover classes over Europe for the period 1989–2018. Our study is the first to analyze distinct seasonal, regional, and land-cover-specific analyses over the entire Europe at 1 km spatial resolution over 30 years. Our results show varying trends for different regions and land cover classes, and reveal that the individual land cover classes have highly different seasonal NDVI trends within different regions in Europe. This confirms the importance of including a combination of both land cover information and biogeographical regions for the analysis of vegetation trends in a large study area with diverse vegetation, such as Europe. The analyses at such a level of detail have been possible based on the recently developed long-term TIMELINE NDVI time-series for Europe at 1 km spatial resolution. Fig. 10 provides a comparison of the pixel size of 1 km TIMELINE NDVI data [see Fig. 10(a)] with data at 4 and 8 km spatial resolution, comparable to the resolution of other available global AVHRR NDVI time-series (e.g., [34], [66], [67], [68]). It becomes obvious that due to the highly fragmented landscapes, which are typical for Europe, the availability of long NDVI time-series at 1 km spatial resolution is a great advantage for meaningful land cover-specific trend analyses.

The large differences among seasons prove that it is important to analyze individual seasons separately and that this provides valuable additional information compared to using the annual mean only. The seasons are defined to the standard definition of three-month periods over Europe. Varying dates of actual start and end of seasons, for e.g., more northern or southern regions, is accounted for by analyzing biogeographical regions separately.

B. Comparison to NDVI Trends From Other Studies

The distribution of areas with positive/negative trends corresponds to the results of previous studies, which also show a general greening of vegetation in Europe but negative trends in parts of the Mediterranean and the Steppic regions (e.g., [24], [26], [29], [69]). Focusing on Europe, for example, Julien et al. [30] reported an NDVI decrease in arid and semiarid areas including southern Spain, and an increase in temperate areas of western and central Europe, especially in the Continental region. He et al. [31] reported an increasing NDVI for large parts of Europe but found negative trends north of the Black Sea and Caspian Sea. These areas lie within the Steppic region, for which we also obtained negative NDVI trends in summer and autumn.

Trends for different land cover classes have rarely been analyzed on European scale before. One study by Vicente-Serrano et al. [70] analyzed NDVI trends in Spain for the period 1981–2014. At an annual scale, changes were positive for all land cover classes. Coniferous forests showed a stronger increase than deciduous and mixed forests and a comparable amount of change to shrubs and pastures. In our study, we observe a higher NDVI increase for broadleaf forest, compared to the other forest types

Fig. 9. Strength of the relation between the climate drivers and the NDVI for areas with significant NDVI trends in the period 1989–2018. The diagrams give the strength of the influence measured by the MCI on the four most prevalent land cover classes (RC: Rain-fed cropland; BF: Broadleaf forest; NF: Needleleaf forest; GL: grassland) separated for areas with significant negative and significant positive NDVI trends for spring, summer, and autumn within each of the biogeographical regions.

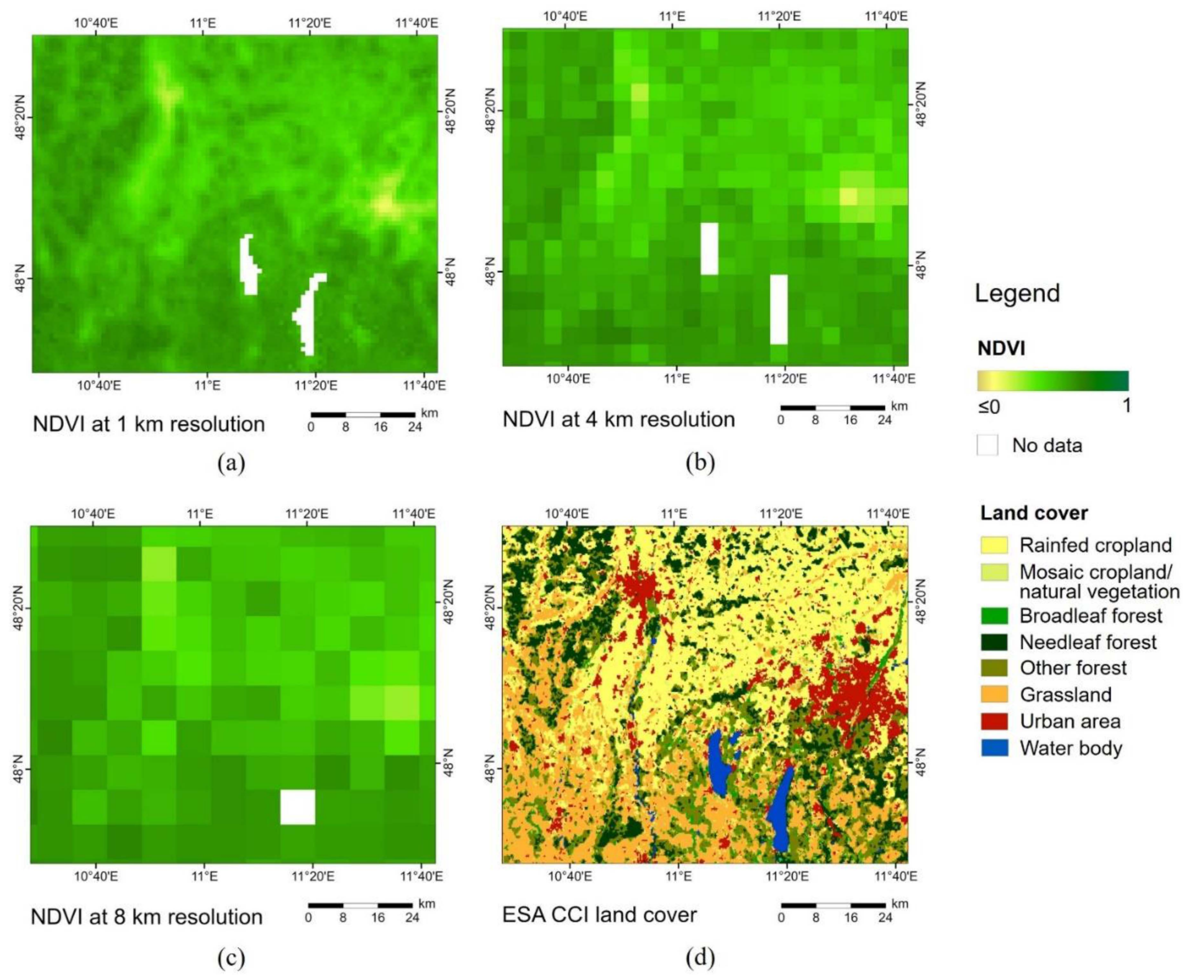

Fig. 10. Comparison of the pixel size of NDVI data at 1 km, 4 km, and 8 km spatial resolution for a subset area in southern Germany with (a) TIMELINE NDVI data (mean annual NDVI) at 1 km resolution, (b) resampled NDVI data with 4 km resolution, (c) resampled NDVI data with 8 km resolution, and (d) land cover from ESA CCI [45].

in the Mediterranean region (see Fig. 5). Consistent with [70], we also find that differences between land cover classes are least pronounced in spring. Vicente-Serrano et al. [70] also analyzed the percentage of surface area impacted by significant trends ($p<0.05$). Their results, for e.g., irrigated land, shrubs, and forest classes, are comparable to our results for the Mediterranean region. Although the study for comparison covers only a small part of the entire study area, the large agreement suggests that the results of our study are reliable, especially as the comparison to other studies on NDVI trends also showed good agreement in the general distribution of positive/negative NDVI trends over Europe (e.g., [24], [26], [29], [69]).

C. Discussion of Regional and Land Cover-Specific Variation of Seasonal NDVI Trends Over Europe

Regarding the NDVI trends for different seasons, we observed a generally stronger increase of NDVI in spring and autumn compared to summer. This might be explained by changes in seasonality, with earlier greening in spring and delayed senescence in autumn. Trends toward a longer growing season in large parts of central and eastern Europe have been reported by several studies such as [24], [22], and [71]. The results of our study also confirm that temperature plays an important role in increasing NDVI in spring.

The comparatively small NDVI increase in summer might also be influenced by a limitation of the vegetation index, as NDVI is prone to saturation. Its sensitivity decreases with increasing leaf area index (LAI) (e.g., [72], [73], [74]). Thus, analyses based on NDVI might underestimate the vegetation trend in summer for areas with dense vegetation canopy and high LAI.

The analyses for the individual regions show clear differences and regional patterns, e.g., regarding differences between seasons. For future studies, additional analyses for smaller regions would be of interest, e.g., in the Mediterranean. Within this region, we observe different and even opposite NDVI trends in summer for the western (Iberian Peninsula) and eastern part (Greece, Türkiye).

A known limit for the analysis of NDVI observations in Arctic and Boreal zones is presence of snow cover, which decreases the values of vegetation indices such as NDVI [75],

[76]. A previous study on snow cover duration (SCD) reported decreasing early SCD (autumn–winter) for areas in the Boreal and Steppic regions [77]. For the late SCD (winter–spring), trends were patchy with both negative and positive trends over Europe [77]. Another publication reported significant negative SCD trends mainly for the Baltic sea region (especially Baltic states) for both early and late SCD [78]. Changes in SCD are not relevant for most of our study area and do not affect the reliability of the results. We do not observe outstanding increasing NDVI trends in the areas possibly affected. However, for more detailed analyses in the Boreal region, focusing, e.g., on the Baltic state, a combined analysis of NDVI and snow cover data, which are also available from the TIMELINE project [79], is recommended.

A general observation from the land-cover-specific analyses is that broadleaf forest shows the largest area with significant positive NDVI trends for all seasons over Europe. Moreover, all three forest classes show very small areas with significant negative trends. The largest percentages of areas with negative trends can be observed for grassland and sparse vegetation in summer, as well as for sparse vegetation and rain-fed cropland in autumn. These are classes that have relatively little biomass and woody vegetation parts in order to store humidity, and hence are especially vulnerable to increasing temperatures and VPD. Differing observations between irrigated cropland and natural herbaceous vegetation, especially in summer, can likely be attributed to human influence on water availability on intensively farmed irrigated areas. Mosaic landscapes generally have fewer negative trends than, for example, cropland and grassland. This indicates that heterogeneous landscapes may be able to cope better with heat and drought.

D. Discussion of Seasonal NDVI Drivers

Considering the analyzed NDVI drivers, this study revealed spatially and seasonally heterogeneous patterns of the climate drivers between 1989 and 2018. In spring, the NDVI was found to be primarily controlled by temperature over a large area in central Europe, especially in the Alpine (Carpathians), Black Sea, Southwest of Boreal, and Continental biogeographic regions. This positive coupling between the NDVI and temperature indicates a strong influence of warming temperatures on the green up of vegetation in these biogeographic regions. Consistent with this, Wang et al. [80] identified a significant positive partial correlation between temperature and the vegetation green-up in parts of the Alpine, Boreal, and Continental biogeographic regions. Also, Wu et al. [37] evaluated the response of the NDVI to climate variables between 1982 and 2008 at an annual scale and reported positive correlations between temperature and the NDVI for large parts of Europe. In this context, Higgins et al. [81] suggested that temperature and moisture are among the variables that explain most of the NDVI variability.

In addition to temperature, Yuan et al. [52] also emphasized the role of atmospheric CO_2 and VPD as important contributors to the variability of the NDVI. In fact, VPD was found to be an important driver of the NDVI over Europe in our study. More specifically, our analysis revealed a predominantly negative coupling between VPD and the NDVI over the Mediterranean and Steppic region during spring, summer, and autumn. For comparison, Yuan et al. [52] calculated the correlation between multiple vegetation indices and VPD between 1982 and 2015 at annual scale; however, while the identified patterns for the NDVI in their study do not exactly match the reported patterns of this study, the patterns match those calculated for the LAI. It should be noted that a comparison of results between studies is challenging due to differences in the used datasets, investigated periods, and used methods.

Moreover, the identified positive coupling between precipitation and the NDVI over the Mediterranean during summer, in particular over the Iberian Peninsula, as well as over large areas of the Steppic region in summer and autumn, likely describes a negative influence. Similar findings for the relation between precipitation and the NDVI were reported by Zhao et al. [82]. The authors analyzed drivers of the NDVI for the growing season between 1982 and 2013 and identified significant positive correlations between precipitation and the NDVI over the Western and Eastern Mediterranean and the Steppic region. However, Zhao et al. [82] did not identify a positive correlation between temperature and the NDVI over large parts of the Continental region as we found in this study. In fact, they found a positive correlation between temperature and the NDVI only over northern areas of Europe, including parts of the Arctic and Boreal region. These contrasting findings might be explained by differences in the considered seasons and studied periods.

Considering the temporal lags of the seasonal NDVI driver analysis, most of the significant causal links were found to have a lag of one month. However, at a temporal lag of three months, temperature and VPD were found to have a maximum influence over some regions of the Anatolian, Mediterranean, and Steppic. In comparison, Wu et al. [37] reported a temporal lag of 0 for the relation between the NDVI and temperature over most parts of Europe. However, in parts of the Anatolian, Mediterranean, and Steppic, the temporal lag was at up to three months as well. In case of precipitation, the authors suggested a temporal lag larger than one month for most parts of Europe.

E. Impact of Climate Drivers on European Vegetation

The analysis of the strength of influence of the climate drivers in areas with significant NDVI trends performed in this study revealed varying impacts for different biogeographical regions and seasons. In several regions (Continental, Pannonian, Steppic, Black Sea, Anatolian, and Alpine), positive NDVI trends in spring are strongly influenced by increasing temperature. Decreasing NDVI in spring can for some regions be related to decreasing VPD (Continental, Boreal, Steppic, Anatolian, and Alpine). Decreasing NDVI in summer and autumn in the Mediterranean, Steppic, and Anatolian regions are mainly influenced by decreasing precipitation but are also related to solar radiation (Mediterranean) and VPD (Steppic and Anatolian).

These results confirm that increasing temperatures in spring lead to earlier and/or increasing vegetation activity in several regions over central Europe. On the other hand, in southern and eastern Europe decreasing NDVI trends in summer (Mediterranean/Iberian Peninsula, and Anatolian) and autumn (Mediterranean/Iberian Peninsula and Steppic) are influenced by decreasing precipitation but also increasing solar radiation and/or VPD, e.g., in the Mediterranean, Steppic, and Anatolian regions. These differentiated analyses are important in order to understand varying effects of climate change on European vegetation. The analyses have shown that different biomes react sensitively to different climatic conditions and weather. Such detailed analyses have now been carried out for the whole of Europe for the first time.

Climate change in Europe is expected to lead to further rising temperatures. This study showed that temperature influenced vegetation growth in spring with a positive coupling over all regions during the last three decades. Thus, future temperature increase might strengthen already existing trends toward increased vegetation growth in spring in Europe. More irregular precipitation patterns, however, might have a negative influence especially in the Mediterranean in summer and autumn, but also in the Steppic region in autumn and in the Anatolian region in summer as vegetation growth in these regions shows to be influenced by precipitation over the past 30 years. Climate change is also predicted to increase the importance of VPD in plant growth [83]. As our study shows, higher VPD in the past led to an increase in NDVI in spring for the Alpine, Arctic, and Boreal regions but to a decrease in other regions across Europe in summer and autumn. Solar radiation influenced summer NDVI in the Mediterranean and most strongly in the Iberian Peninsula where increasing solar radiation led to a decrease in vegetation growth. Thus, increasing solar radiation in combination with decreasing precipitation can be expected to intensify the risk of droughts, especially in this area in future.

F. Outlook and Future Research Potential

The TIMELINE NDVI product offers the unique ability to analyze a time-series of almost 40 years over Europe with a spatial resolution of 1 km and a temporal resolution of up to one day. In this study, we analyzed seasonal trends based on the monthly NDVI composites. Several additional information products can be derived from the TIMELINE NDVI data, such as anomalies or phenological information, which can assist to further understand ongoing vegetation change and dynamics. Application of recent methods, such as advanced time-series reconstruction (e.g., [84]) or additional trend detection methods (e.g., [85]) might allow to address further research questions.

There is also a lot of potential in the dataset, e.g., in combination with other TIMELINE data, such as land surface temperature or snow cover. Also, combination with other freely available data sources, including information on soil moisture, heat waves, or deforestation, would allow to tackle additional research topics.

Further future research potential exists in the application of multisources data and comparing the conclusions obtained from different data sources. Fusion of AVHRR and MODIS NDVI (e.g., [86]) or Landsat data can be used to generate global long-term NDVI data at higher spatial resolution compared to previously available global datasets. This, however, requires additional harmonization, sophisticated downscaling, and validation to generate reliable time-series. Comparison of observations from different data sources can support quality assessment and confirm and reinforce trends and conclusions obtained.

The TIMELINE NDVI product is currently subject to further development. Data processing for the extension of the time-series to more recent years is ongoing, allowing for the analysis of an even longer NDVI time-series in future.

VII. Conclusion

In this study, we conducted the first detailed causal exploration of NDVI drivers for different biogeographical regions and land covers at a seasonal temporal scale for Europe. Our results reinforce the previously reported general greening of vegetation in Europe over the last decades. However, the detailed spatial and regional analyses reveal that this greening is not pervasive and that some areas experienced seasonal decrease in NDVI over the 30-year period from 1989 to 2018, e.g., within the Steppic, Anatolian, and Mediterranean regions. Our results also reveal differences between seasons. For most regions, NDVI trends are lowest in summer. The trends for the different biogeographical regions indicate that regions in western and central Europe (Atlantic, Continental, Mediterranean, and Pannonian) tend to show a stronger positive NDVI trend in autumn compared to spring and summer. In contrast, the regions toward the South-East (Steppic, Black Sea, and Anatolian) have a stronger positive NDVI trend in spring and lower positive or negative NDVI trends in summer and autumn. These results confirm that seasonally differentiated analyses, as performed in this study, are required to capture the various differences in vegetation growth.

Moreover, individual land cover classes within biogeographical regions showed strong differences both in the strength of seasonal NDVI trends and in the percentage of area affected. Also, areas with the same land cover show very different behavior in the different zones. These results corroborate the relevance of including and combining both spatial information about land cover distribution and discrete geographical regions for the analysis of long-term NDVI trends over large and diverse study areas such as Europe.

Regarding the influence of climatic drivers on the NDVI, our study disclosed several major findings. In spring, the NDVI was primarily controlled by temperature (positive coupling) in the biogeographic regions such as Continental, Southwest of Boreal, Black Sea, and Alpine (Carpathians), especially the areas with positive NDVI trends were influenced by increasing temperatures in spring in several regions. Regarding the influence of VPD, our analysis revealed mostly a negative coupling with the NDVI in parts of the Mediterranean, Anatolian, and Steppic regions during spring, summer, and autumn. For areas with negative NDVI trends, especially in the northern Steppic, eastern Continental, and Boreal, in contrast, a positive coupling to VPD was observed in spring. A coupling between decreasing precipitation and decreasing NDVI was identified over the Mediterranean, in particular over the Iberian Peninsula, and the Anatolian region during summer, and in the Steppic and Mediterranean regions in autumn. These trends are expected to aggravate under ongoing climate change.

Our study is based upon the recently developed TIMELINE NDVI product providing a consistent time-series for more than 30 years covering entire Europe at 1 km spatial resolution. Combined with a land cover data set, this allowed for European-wide NDVI analyses at a level of detail not available before. The results of our study significantly contribute to further understand the vegetation activity dynamics over Europe.

APPENDIX

The appendix contains Tables I and II, and Figs. 11, 12, 13, and 14

TABLE I
GROUPED LAND COVER CLASSES USED WITHIN THIS STUDY

LC name	LC short name	Area with stable vegetated land cover in study area [%]	ESA-CCI classes included
Rain-fed cropland	RC	31.5	10: Cropland, rain-fed 11: Herbaceous cover 12: Tree or shrub cover
Irrigated cropland	IC	1.1	20: Cropland, irrigated, or post flooding
Mosaic cropland/natural	MC	4.9	30: Mosaic cropland (>50%) / natural vegetation (tree, shrub, herbaceous cover) (<50%) 40: Mosaic natural vegetation (tree, shrub, herbaceous cover) (>50%) / cropland (<50%)
Broadleaf forest	BF	10.8	60: Tree cover, broadleaved, deciduous, closed to open (>15%) 61: Tree cover, broadleaved, deciduous, closed (>40%) 62: Tree cover, broadleaved, deciduous, open (15-40%)
Needleleaf forest	NF	15.5	70: Tree cover, needleleaved, evergreen, closed to open (>15%) 71: Tree cover, needleleaved, evergreen, closed (>40%) 72: Tree cover, needleleaved, evergreen, open (15-40%)
Other forest	OF	8.1	50: Tree cover, broadleaved, evergreen, closed to open (>15%) 80: Tree cover, needleleaved, deciduous, closed to open (>15%) 81: Tree cover, needleleaved, deciduous, closed (>40%) 82: Tree cover, needleleaved, deciduous, open (15-40%) 90: Tree cover, mixed leaf type (broadleaved and needleleaved) 100: Mosaic tree and shrub (>50%) / herbaceous cover (<50%)
Shrubland	SL	1.2	120: Shrubland 121: Evergreen shrubland 122: Deciduous shrubland
Grassland	GL	8.2	130: Grassland 110: Mosaic herbaceous cover (>50%) / tree and shrub (<50%)
Sparse vegetation	SV	2.1	140: Lichens and mosses 150: Sparse vegetation (tree, shrub, herbaceous cover) (<15%) 151: Sparse tree (<15%) 152: Sparse shrub (<15%) 153: Sparse herbaceous cover (<15%)
Flooded area	FA	2.3	160: Tree cover, flooded, fresh, or brackish water 170: Tree cover, flooded, saline water 180: Shrub or herbaceous cover flooded
Urban area	NSV (no stable vegetation)	-	190: Urban areas
Bare area		-	200: Bare areas, 201: Consolidated bare areas, 202: unconsolidated bare areas
Water body		-	210: Water bodies
Snow and ice		-	220: Permanent snow and ice
No stable LC		-	-

The first to third columns give the land cover (LC) class names and the percentual area with stable land cover in the study area for the vegetated land cover classes. The fourth column lists the ESA-CCI classes included for each grouped LC class.

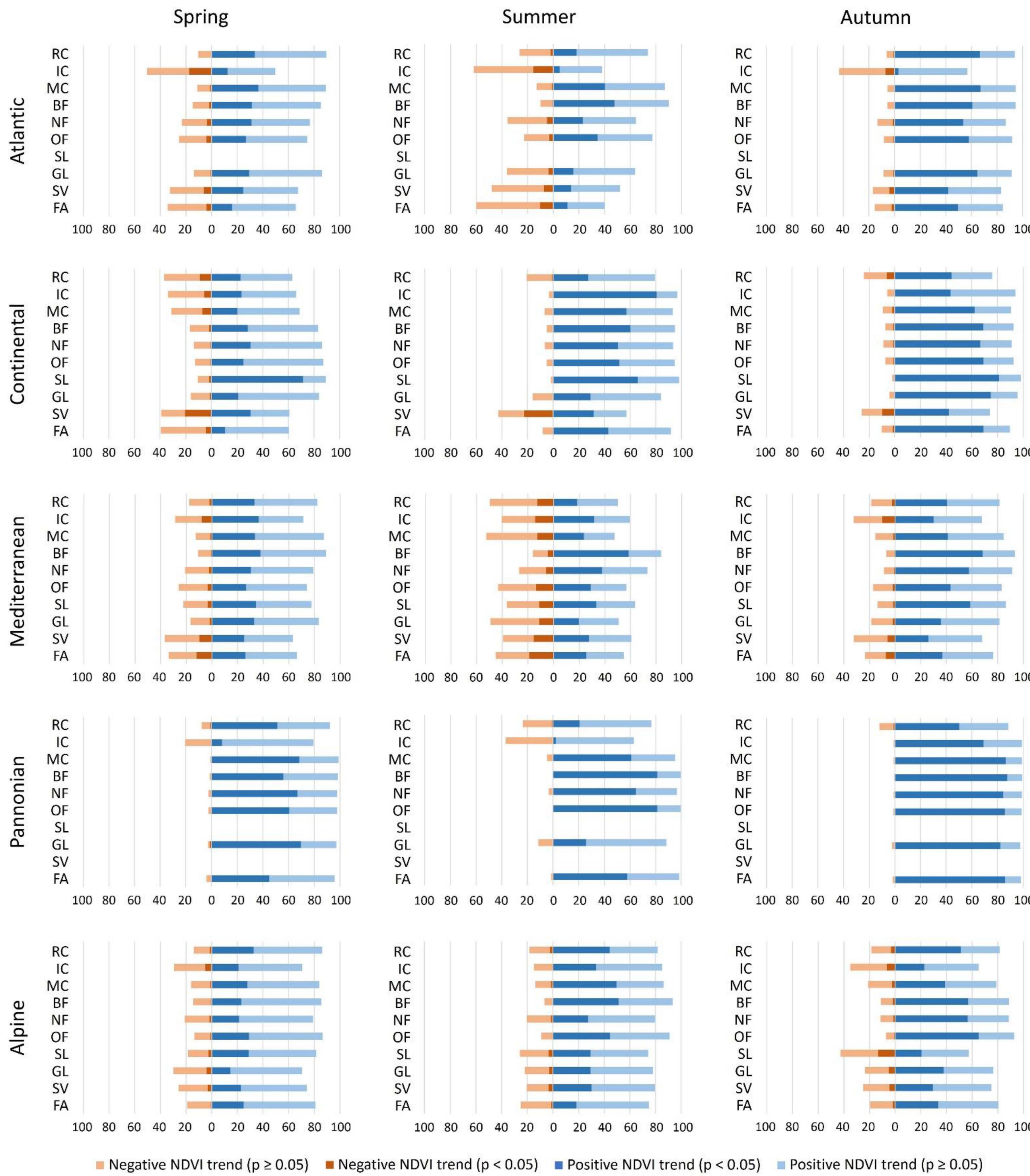

Fig. 11. Percent area with negative (red) or positive (blue) NDVI trends for individual land cover classes within the biogeographical regions for spring (left), summer (center), and autumn (right). Different intensities of color differentiate between significant ($p<0.05$, dark red and blue) and nonsignificant ($p\geq0.05$, bright red and blue) trends. The land cover classes are RC: Rain-fed cropland; IC: Irrigated cropland; MC: Mosaic cropland/natural; BF: Broadleaf forest; NF: Needleleaf forest; OF: Other forest; SL: Shrubland; GL: Grassland; SV: Sparse vegetation; FA: Flooded area.

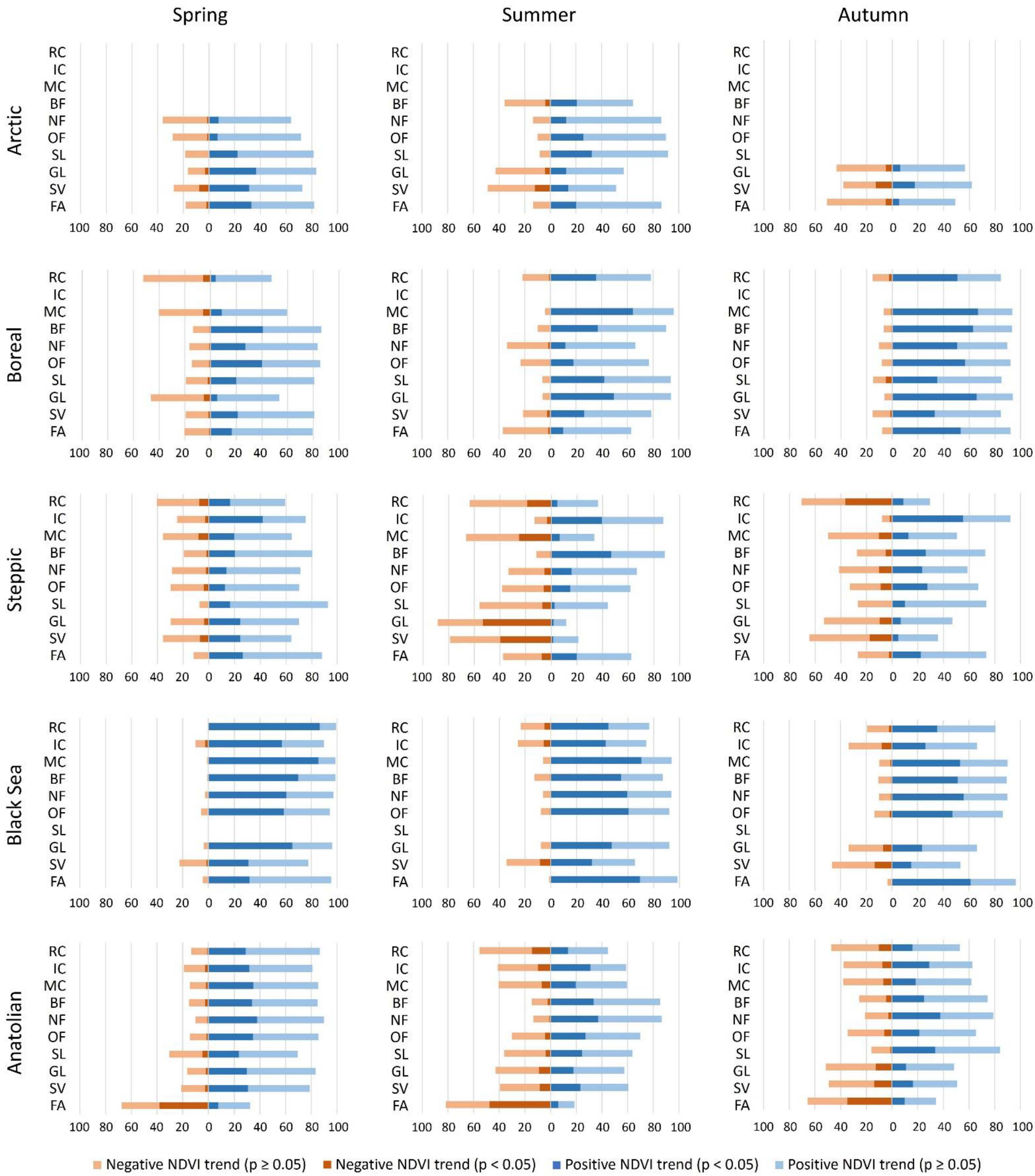

Fig. 11. *(Continued.)*

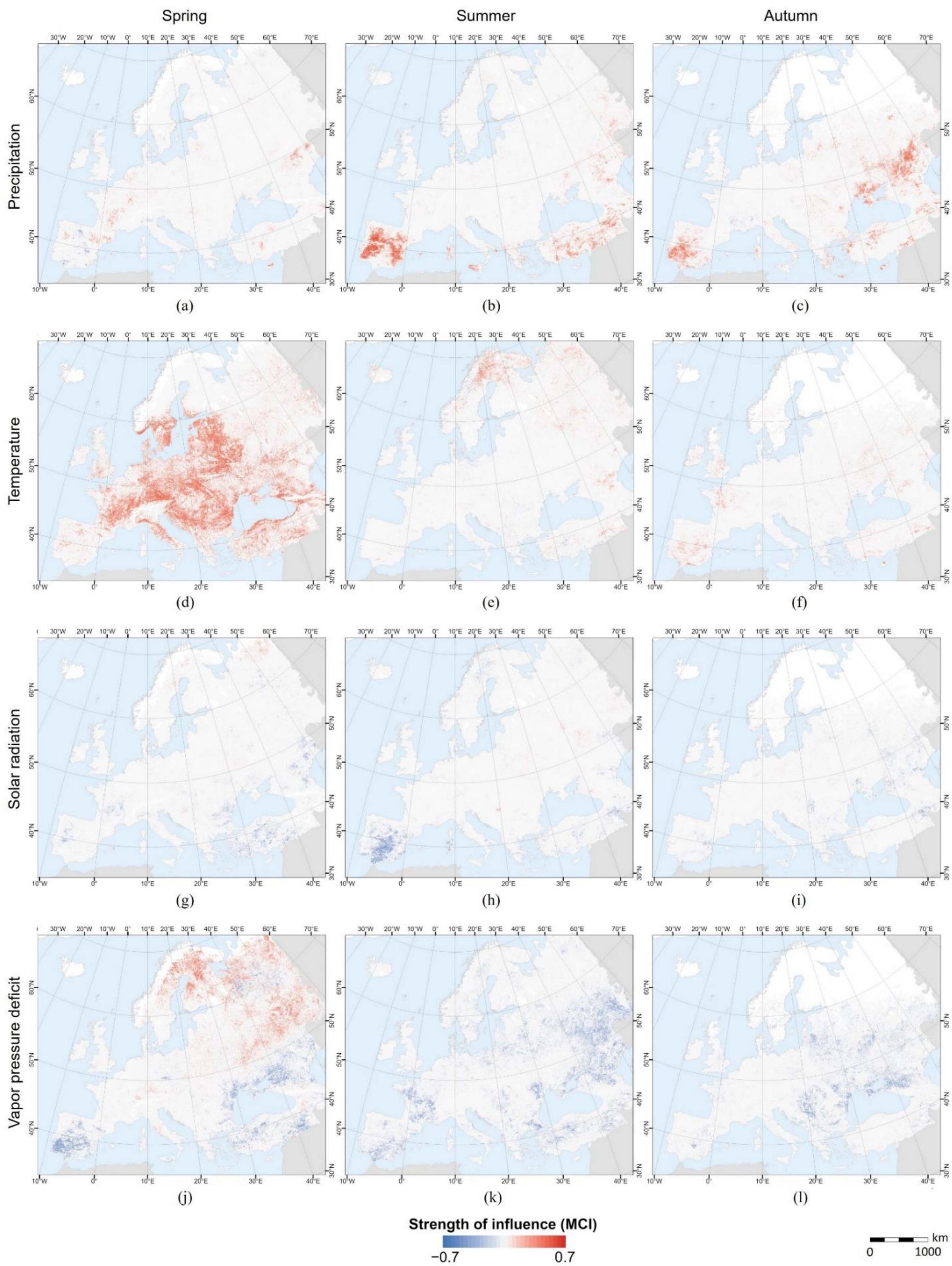

Fig. 12. Strength of the relation between the climate drivers and the NDVI per season separately for the four climate variables. The strength of the influence is measured by the MCI test, which is the partial correlation coefficient. Pixels in light gray color have no causal link. Pixels in white were excluded from the analysis due to a low NDVI value or data availability.

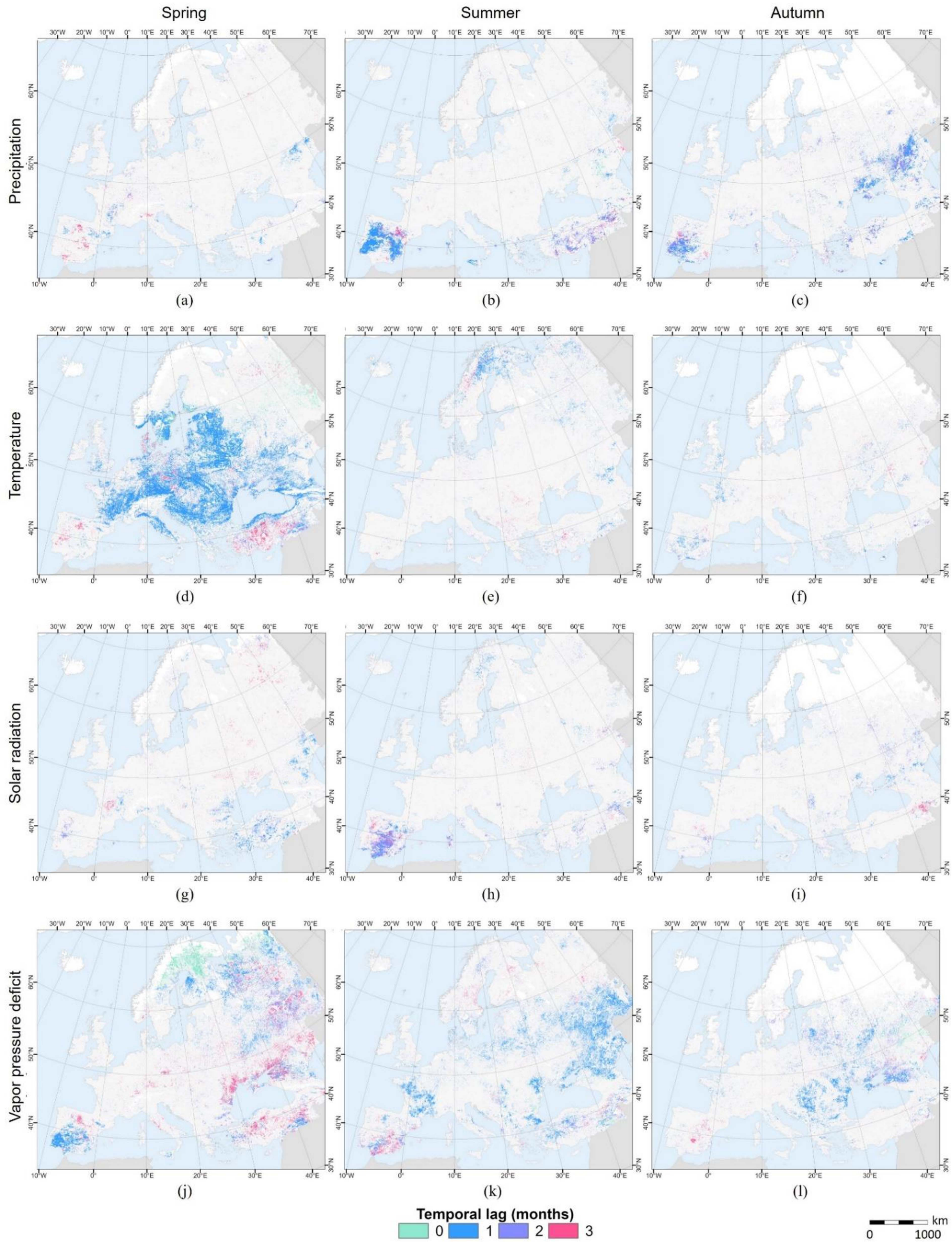

Fig. 13. Temporal lags for the estimated relation between the climate drivers and the NDVI separately for the four climate variables. The temporal lags are measured in months. Pixels in light gray color have no causal link. Pixels in white were excluded from the analysis due to a low NDVI value or data availability.

Fig. 14. Strength of the relation between the climate drivers (temperature, precipitation, solar radiation, and VPD) and the NDVI for the three seasons (spring, summer, and autumn) for the period 1989–2018. The diagrams give the strength of the influence measured by the MCI on individual land cover classes within each of the biogeographical regions. The region abbreviations are Alp: Alpine, Ana: Anatolian, Arc: Arctic, Atl: Atlantic, Bla: Black sea, Bor: Boreal, Con: Continental, Med: Mediterranean, Pan: Pannonian, and Ste: Steppic.

TABLE II
BIOGEOGRAPHICAL REGIONS IN EUROPE AND THEIR AREA COVERAGE

			Area with stable land cover in region [%]									
Name of region	Short name	Area [1000 km²]	RC	IC	MC	BF	NF	OF	SL	GL	SV	FA
Alpine	Alp	944.5	5.7	0.1	2.8	21.6	18.5	9.9	1.2	12.2	7.8	3.2
Anatolian	Ana	437.3	37.1	11.6	12.0	0.2	0.8	7.0	0.6	13.0	4.7	0.4
Arctic	Arc	243.2	0.0	0.0	0.0	0.1	9.4	2.5	19.7	10.0	20.8	13.4
Atlantic	Atl	861.4	36.2	0.0	2.0	7.3	5.4	1.9	0.0	26.7	1.1	2.9
BlackSea	Bla	139.7	13.4	1.6	8.6	31.9	10.2	10.5	0.0	5.4	0.4	0.9
Boreal	Bor	2839.6	7.2	0.0	3.2	14.5	38.2	15.6	0.2	0.8	0.2	4.7
Continental	Con	2558.8	52.3	0.2	5.8	11.7	7.7	4.4	0.0	5.0	0.0	0.2
Mediterranean	Med	1192.9	36.4	4.5	8.0	7.1	7.5	11.2	4.5	4.0	1.2	0.5
Pannonian	Pan	151.2	73.7	0.1	0.5	10.4	0.6	1.0	0.0	4.6	0.0	0.3
Steppic	Ste	1248.0	56.8	0.0	6.1	2.0	0.5	0.3	0.2	18.4	3.6	0.9

In addition, the percentage of area with stable land cover for individual land cover classes (see Table I) within each biogeographical region is given. The land cover classes are RC: Rain-fed Cropland; IC: Irrigated Cropland; MC: Mosaic Cropland/Natural; BF: Broadleaf Forest; NF: Needleleaf Forest; OF: Other Forest; SL: Shrubland; GL: Grassland; SV: Sparse Vegetation; FA: Flooded Area.

REFERENCES

[1] J. A. Gamon, B. Somers, Z. Malenovský, E. M. Middleton, U. Rascher, and M. E. Schaepman, "Assessing vegetation function with imaging spectroscopy," *Surv. Geophys.*, vol. 40, no. 3, pp. 489–513, May 2019, doi: 10.1007/s10712-019-09511-5.

[2] J. L. Chen, Z. F. Shao, X. J. Deng, X. Huang, and C. Y. Dang, "Vegetation as the catalyst for water circulation on global terrestrial ecosystem," *Sci. Total Environ.*, vol. 895, Oct. 2023, Art. no. 165071, doi: 10.1016/j.scitotenv.2023.165071.

[3] H. Mooney et al., "Biodiversity, climate change, and ecosystem services," *Curr. Opin. Environ. Sustain.*, vol. 1, no. 1, pp. 46–54, Oct. 2009, doi: 10.1016/j.cosust.2009.07.006.

[4] M. Zhao, A. Geruo, J. E. Zhang, I. Velicogna, C. Z. Liang, and Z. Y. Li, "Ecological restoration impact on total terrestrial water storage," *Nature Sustain.*, vol. 4, no. 1, pp. 56–U85, Jan. 2021, doi: 10.1038/s41893-020-00600-7.

[5] H. H. Qiu, J. Y. Zhang, H. R. Han, X. Q. Cheng, and F. F. Kang, "Study on the impact of vegetation change on ecosystem services in the loess plateau, China," *Ecol. Indicators*, vol. 154, Oct. 2023, Art. no. 110812, doi: 10.1016/j.ecolind.2023.110812.

[6] L. G. Simpson and D. B. Botkin, "Vegetation, the global carbon-cycle, and global measures," *ACS Symp. Ser.*, vol. 483, pp. 413–425, 1992.

[7] C. Eisfelder, C. Kuenzer, and S. Dech, "Derivation of biomass information for semi-arid areas using remote-sensing data," *Int. J. Remote Sens.*, vol. 33, no. 9, pp. 2937–2984, 2012, doi: 10.1080/01431161.2011.620034.

[8] Z. Y. Sha et al., "The global carbon sink potential of terrestrial vegetation can be increased substantially by optimal land management," *Commun. Earth Environ.*, vol. 3, no. 1, Jan. 2022, Art. no. 8, doi: 10.1038/s43247-021-00333-1.

[9] A. Ayanlade, C. M. Sergi, P. Di Carlo, O. S. Ayanlade, and D. T. Agbalajobi, "When climate turns nasty, what are recent and future implications? Ecological and human health review of climate change impacts," *Curr. Climate Change Rep.*, vol. 6, no. 3, pp. 55–65, Sep. 2020, doi: 10.1007/s40641-020-00158-8.

[10] K. Huang et al., "Enhanced peak growth of global vegetation and its key mechanisms," *Nature Ecol. Evol.*, vol. 2, no. 12, pp. 1897–1905, Dec. 2018, doi: 10.1038/s41559-018-0714-0.

[11] S. F. Jin, L. X. Wang, and X. D. Yan, "Climate change adaptation and disaster risk assessments: A preface," *Phys. Chem. Earth*, vol. 120, no. 2, Dec. 2020, Art. no. 102920, doi: 10.1016/j.pce.2020.102920.

[12] J. Tollefson, "Earth is warmer than it's been in 125,000 years, says landmark climate report," *Nature*, vol. 596, no. 7871, pp. 171–172, Aug. 2021, doi: 10.1038/d41586-021-02179-1.

[13] S. Mohanty and B. P. Mohanty, "Global climate change: A cause of concern," *Nat. Acad. Sci. Lett.-India*, vol. 32, no. 5/6, pp. 149–156, 2009.

[14] A. D. Richardson, T. F. Keenan, M. Migliavacca, Y. Ryu, O. Sonnentag, and M. Toomey, "Climate change, phenology, and phenological control of vegetation feedbacks to the climate system," *Agricultural Forest Meteorol.*, vol. 169, pp. 156–173, Feb. 2013, doi: 10.1016/j.agrformet.2012.09.012.

[15] H. S. Gu et al., "Warming-induced increase in carbon uptake is linked to earlier spring phenology in temperate and boreal forests," *Nature Commun.*, vol. 13, no. 1, Jun. 2022, Art. no. 3698, doi: 10.1038/s41467-022-31496-w.

[16] Eur. Commission, "2023 European state of the climate report confirms alarming trend of climate change impacts on our continent," 2024. Accessed: Jul. 24, 2024. [Online]. Available: https://defence-industry-space.ec.europa.eu/2023-European-state-climate-report-confirms-alarming-trend-climate-change-impacts-our-continent-2024-04-22_en

[17] Eur. Commission et al., "Climate change impacts and adaptation in Europe – JRC PESETA IV final report," Pub. Office Eur. Union, Tech. Rep. JRC119178, 2020.

[18] G. Lieberherr and S. Wunderle, "Lake surface water temperature derived from 35 years of AVHRR sensor data for European lakes," *Remote Sens.-Basel*, vol. 10, no. 7, Jul. 2018, Art. no. 990, doi: 10.3390/rs10070990.

[19] S. Dech et al., "Potential and challenges of harmonizing 40 years of AVHRR data: The TIMELINE experience," *Remote Sens.-Basel*, vol. 13, no. 18, Sep. 2021, Art. no. 3618, doi: 10.3390/rs13183618.

[20] S. Huang, L. N. Tang, J. P. Hupy, Y. Wang, and G. F. Shao, "A commentary review on the use of normalized difference vegetation index (NDVI) in the era of popular remote sensing," *J. Forestry Res.*, vol. 32, no. 1, pp. 1–6, Feb. 2021, doi: 10.1007/s11676-020-01155-1.

[21] J. Xiao and A. Moody, "Geographical distribution of global greening trends and their climatic correlates: 1982-1998," *Int. J. Remote Sens.*, vol. 26, no. 11, pp. 2371–2390, Jun. 2005, doi: 10.1080/01431160500033682.

[22] Y. Julien and J. A. Sobrino, "Global land surface phenology trends from GIMMS database," *Int. J. Remote Sens.*, vol. 30, no. 13, pp. 3495–3513, 2009, doi: 10.1080/01431160802562255.

[23] H. E. Beck, T. R. McVicar, A. I. J. M. van Dijk, J. Schellekens, R. A. M. de Jeu, and L. A. Bruijnzeel, "Global evaluation of four AVHRR-NDVI data sets: Intercomparison and assessment against landsat imagery," *Remote Sens. Environ.*, vol. 115, no. 10, pp. 2547–2563, Oct. 2011, doi: 10.1016/j.rse.2011.05.012.

[24] R. de Jong, S. de Bruin, A. de Wit, M. E. Schaepman, and D. L. Dent, "Analysis of monotonic greening and browning trends from global NDVI time-series," *Remote Sens. Environ.*, vol. 115, no. 2, pp. 692–702, Feb. 2011, doi: 10.1016/j.rse.2010.10.011.

[25] J. A. Sobrino and Y. Julien, "Global trends in NDVI-derived parameters obtained from GIMMS data," *Int. J. Remote Sens.*, vol. 32, no. 15, pp. 4267–4279, 2011, doi: 10.1080/01431161.2010.486414.

[26] R. Fensholt and S. R. Proud, "Evaluation of Earth observation based global long term vegetation trends - comparing GIMMS and MODIS global NDVI time series," *Remote Sens. Environ.*, vol. 119, pp. 131–147, Apr. 16 2012, doi: 10.1016/j.rse.2011.12.015.

[27] J. R. Eastman, F. Sangermano, E. A. Machado, J. Rogan, and A. Anyamba, "Global trends in seasonality of normalized difference vegetation index (NDVI), 1982-2011," *Remote Sens.-Basel*, vol. 5, no. 10, pp. 4799–4818, Oct. 2013, doi: 10.3390/rs5104799.

[28] Y. Liu, Y. Li, S. Li, and S. Motesharrei, "Spatial and temporal patterns of global NDVI trends: Correlations with climate and human factors," *Remote Sens.*, vol. 7, no. 10, pp. 13233–13250, 2015, doi: 10.3390/rs71013233.

[29] Y. L. Zhang, C. H. Song, L. E. Band, G. Sun, and J. X. Li, "Reanalysis of global terrestrial vegetation trends from MODIS products: Browning or greening?," *Remote Sens. Environ.*, vol. 191, pp. 145–155, Mar. 15 2017, doi: 10.1016/j.rse.2016.12.018.

[30] Y. Julien, J. A. Sobrino, and W. Verhoef, "Changes in land surface temperatures and NDVI values over Europe between 1982 and 1999," *Remote Sens. Environ.*, vol. 103, no. 1, pp. 43–55, Jul. 15, 2006, doi: 10.1016/j.rse.2006.03.011.

[31] Q. He et al., "Impact of the North Sea-Caspian pattern on meteorological drought and vegetation response over diverging environmental systems in western Eurasia," *Ecohydrology*, vol. 15, no. 5, Jul. 2022, Art. no. e2446, doi: 10.1002/eco.2446.

[32] S. Asam, C. Eisfelder, A. Hirner, P. Reiners, S. Holzwarth, and M. Bachmann, "AVHRR NDVI compositing method comparison and generation of multi-decadal time series-A TIMELINE thematic processor," *Remote Sens.-Basel*, vol. 15, no. 6, Mar. 2023, Art. no. 1631, doi: 10.3390/rs15061631.

[33] C. Eisfelder et al., "Seasonal vegetation trends for Europe over 30 years from a novel normalised difference vegetation index (NDVI) time-series-the TIMELINE NDVI product," *Remote Sens.-Basel*, vol. 15, no. 14, Jul. 2023, Art. no. 3616, doi: 10.3390/rs15143616.

[34] E. Vermote and N. C. Program. *NOAA Climate Data Record (CDR) of AVHRR Normalized Difference Vegetation Index (NDVI), Version 5. NOAA National Centers For Environmental Information*. Washington, DC, USA: NOAA National Centers for Environmental Information, 2021. doi: 10.7289/V5ZG6QH9.

[35] J. Xiao and A. Moody, "Geographical distribution of global greening trends and their climatic correlates: 1982–1998," *Int. J. Remote Sens.*, vol. 26, no. 11, pp. 2371–2390, 2008, doi: 10.1080/01431160500033682.

[36] J. Runge, P. Nowack, M. Kretschmer, S. Flaxman, and D. Sejdinovic, "Detecting and quantifying causal associations in large nonlinear time series datasets," *Sci. Adv.*, vol. 5, no. 11, Nov. 2019, Art. no. eaau4996, doi: 10.1126/sciadv.aau4996.

[37] D. Wu et al., "Time-lag effects of global vegetation responses to climate change," *Glob. Change Biol.*, vol. 21, no. 9, pp. 3520–3531, Sep. 2015, doi: 10.1111/gcb.12945.

[38] X. Xie, B. He, L. Guo, C. Miao, and Y. Zhang, "Detecting hotspots of interactions between vegetation greenness and terrestrial water storage using satellite observations," *Remote Sens. Environ.*, vol. 231, 2019, Art. no. 111259, doi: 10.1016/j.rse.2019.111259.

[39] C. Papagiannopoulou, D. G. Miralles, W. A. Dorigo, N. E. C. Verhoest, M. Depoorter, and W. Waegeman, "Vegetation anomalies caused by antecedent precipitation in most of the world," *Environ. Res. Lett.*, vol. 12, no. 7, 2017, Art. no. 074016, doi: 10.1088/1748-9326/aa7145.

[40] J. Runge et al., "Inferring causation from time series in earth system sciences," *Nature Commun.*, vol. 10, no. 1, Jun. 2019, Art. no. 2553, doi: 10.1038/s41467-019-10105-3.

[41] S. Uereyen, F. Bachofer, I. Klein, and C. Kuenzer, "Multi-faceted analyses of seasonal trends and drivers of land surface variables in Indo-Gangetic river basins," *Sci. Total Environ.*, vol. 847, Nov. 2022, Art. no. 157515, doi: 10.1016/j.scitotenv.2022.157515.

[42] S. Uereyen, I. Klein, C. Eisfelder, and C. Kuenzer, "Multivariate analysis of land surface dynamics in central Asia: Patterns of trends and drivers under a changing climate," *GIScience Remote Sens.*, vol. 61, no. 1, 2024, Art. no. 2364461, doi: 10.1080/15481603.2024.2364461.

[43] C. Krich et al., "Estimating causal networks in biosphere–atmosphere interaction with the PCMCI approach," *Biogeosciences*, vol. 17, no. 4, pp. 1033–1061, 2020, doi: 10.5194/bg-17-1033-2020.

[44] EEA, "Biogeographical regions in Europe," 2016. Accessed: Feb. 7, 2024. [Online]. Available: https://www.eea.europa.eu/en/analysis/maps-and-charts/biogeographical-regions-in-europe-2

[45] ESA, "Land cover CCI product user guide version 2. Tech. Rep," 2017. Accessed: Sep. 19, 2024. [Online]. Available: https://maps.elie.ucl.ac.be/CCI/viewer/download/ESACCI-LC-Ph2-PUGv2_2.0.pdf

[46] H. E. Peifer, "About the EEA reference grid," 2011. Accessed: Jun. 30, 2023. [Online]. Available: https://www.eea.europa.eu/data-and-maps/data/eea-reference-grids-2/about-the-eea-reference-grid/eea_reference_grid_v1.pdf/at_download/

[47] EEA, "Datahub: Biogeographical regions," 2024. Accessed: Feb. 7, 2024. [Online]. Available: https://www.eea.europa.eu/en/datahub/datahubitem-view/11db8d14-f167-4cd5-9205-95638dfd9618

[48] J. Muñoz-Sabater, "ERA5-land monthly averaged data from 1950 to present. Copernicus climate change service (C3S) climate data store (CDS)," 2019. Accessed: Feb. 7, 2024. doi: 10.24381/cds.68d2bb30.

[49] M. Bandhauer et al., "Evaluation of daily precipitation analyses in E-OBS (v19.0e) and ERA5 by comparison to regional high-resolution datasets in European regions," *Int. J. Climatol.*, vol. 42, no. 2, pp. 727–747, 2021, doi: 10.1002/joc.7269.

[50] B. McNicholl, Y. H. Lee, A. G. Campbell, and S. Dev, "Evaluating the reliability of air temperature from ERA5 reanalysis data," *IEEE Geosci. Remote Sens. Lett.*, vol. 19, 2022, Art. no. 1004505, doi: 10.1109/lgrs.2021.3137643.

[51] A. Barkhordarian, S. S. Saatchi, A. Behrangi, P. C. Loikith, and C. R. Mechoso, "A recent systematic increase in vapor pressure deficit over tropical south America," *Sci. Rep.*, vol. 9, no. 1, Oct. 019, Art. no. 15331, doi: 10.1038/s41598-019-51857-8.

[52] W. Yuan et al., "Increased atmospheric vapor pressure deficit reduces global vegetation growth," *Sci. Adv.*, vol. 5, no. 8, Aug. 2019, Art. no. eaax1396, doi: 10.1126/sciadv.aax1396.

[53] A. G. Konings, A. P. Williams, and P. Gentine, "Sensitivity of grassland productivity to aridity controlled by stomatal and xylem regulation," *Nature Geosci.*, vol. 10, no. 4, pp. 284–288, 2017, doi: 10.1038/ngeo2903.

[54] H. B. Mann, "Nonparametric tests against trend," *Econometrica*, vol. 13, no. 3, pp. 245–259, 1945, doi: 10.2307/1907187.

[55] M. Kendall, *Rank Correlation Measures*. London, U.K.: Charles Griffin, 1975.

[56] H. Theil, "A rank-invariant method of linear and polynomial regression analysis," *Nederlandse Akademie Wetenchappen A*, vol. 53, pp. 386–392, 1950.

[57] P. K. Sen, "Estimates of the regression coefficient based on Kendall's tau," *J. Amer. Stat. Assoc.*, vol. 63, no. 324, pp. 1379–1389, 1968, doi: 10.1080/01621459.1968.10480934.

[58] X. Y. Guo, H. Y. Zhang, Z. F. Wu, J. J. Zhao, and Z. X. Zhang, "Comparison and evaluation of annual NDVI time series in China derived from the NOAA AVHRR LTDR and terra MODIS MOD13C1 products," *Sensors-Basel*, vol. 17, no. 6, Jun. 2017, Art. no. 1298, doi: 10.3390/s17061298.

[59] K. C. Guay, P. S. A. Beck, L. T. Berner, S. J. Goetz, A. Baccini, and W. Buermann, "Vegetation productivity patterns at high northern latitudes: A multi-sensor satellite data assessment," *Glob. Change Biol.*, vol. 20, no. 10, pp. 3147–3158, Oct. 2014, doi: 10.1111/gcb.12647.

[60] J. Runge, "Discovering contemporaneous and lagged causal relations in autocorrelated nonlinear time series datasets," in *Proc. 36th Conf. Uncertainty Artif. Intell., Proc. Mach. Learn. Res.*, 2020, pp. 1–10. [Online]. Available: http://proceedings.mlr.press/v124/runge20a.html

[61] J. Runge, "Causal network reconstruction from time series: From theoretical assumptions to practical estimation," *Chaos*, vol. 28, no. 7, Jul. 2018, Art. no. 075310, doi: 10.1063/1.5025050.

[62] J. A. Sobrino, J. C. Jiménez-Muñoz, and L. Paolini, "Land surface temperature retrieval from LANDSAT TM 5," *Remote Sens. Environ.*, vol. 90, no. 4, pp. 434–440, Apr. 2004, doi: 10.1016/j.rse.2004.02.003.

[63] A. Zaitunah and F. Sahara, "Mapping and assessment of vegetation cover change and species variation in Medan, north Sumatra," *Heliyon*, vol. 7, no. 7, Jul. 2021, Art. no. e07637, doi: 10.1016/j.heliyon.2021.e07637.

[64] Y. Zeng et al., "Changes in vegetation greenness related to climatic and non-climatic factors in the Sudano-Sahelian region," *Regional Environ. Change*, vol. 23, no. 3, Jun. 2023, Art. no. 92, doi: 10.1007/s10113-023-02084-5.

[65] M. Barben, S. Wunderle, and S. Dupuis, "A 40-year time series of land surface emissivity derived from AVHRR sensors: A Fennoscandian perspective," *Remote Sens.-Basel*, vol. 16, no. 19, 2024, Art. no. 3686, doi: 10.3390/rs16193686.

[66] J. Pedelty et al., "Generating a long-term land data record from the AVHRR and MODIS instruments," in *Proc. IEEE Int. Geosci. Remote Sens. Symp.*, 2007, pp. 1021–1024, doi: 10.1109/Igarss.2007.4422974.

[67] C. J. Tucker et al., "An extended AVHRR 8-km NDVI dataset compatible with MODIS and SPOT vegetation NDVI data," *Int. J. Remote Sens.*, vol. 26, no. 20, pp. 4485–4498, Oct. 2005, doi: 10.1080/01431160500168686.

[68] J. E. Pinzon and C. J. Tucker, "A non-stationary 1981-2012 AVHRR NDVI3g time series," *Remote Sens.-Basel*, vol. 6, no. 8, pp. 6929–6960, Aug. 2014, doi: 10.3390/rs6086929.

[69] Z. Q. Wang et al., "Large discrepancies of global greening: Indication of multi-source remote sensing data," *Glob. Ecol. Conservation*, vol. 34, Apr. 2022, Art. no. e02016, doi: 10.1016/j.gecco.2022.e02016.

[70] S. M. Vicente-Serrano et al., "Vegetation greening in Spain detected from long term data (1981–2015)," *Int. J. Remote Sens.*, vol. 41, no. 5, pp. 1709–1740, Mar. 2020, doi: 10.1080/01431161.2019.1674460.

[71] L. Klimavicius, E. Rimkus, E. Stonevicius, and V. Maciulyte, "Seasonality and long-term trends of NDVI values in different land use types in the eastern part of the Baltic sea basin," *Oceanologia*, vol. 65, no. 1, pp. 171–181, Jan./Mar. 2023, doi: 10.1016/j.oceano.2022.02.007.

[72] S. Tanaka, K. Kawamura, M. Maki, Y. Muramoto, K. Yoshida, and T. Akiyama, "Spectral index for quantifying leaf area index of winter wheat by field hyperspectral measurements: A case study in Gifu prefecture, central Japan," *Remote Sens.-Basel*, vol. 7, pp. 5329–5346, Apr. 2015, doi: 10.3390/rs70505329.

[73] X. Gao, A. R. Huete, W. Ni, and T. Miura, "Optical–biophysical relationships of vegetation spectra without background contamination," *Remote Sens. Environ.*, vol. 74, no. 3, pp. 609–620, Dec. 2000, doi: 10.1016/S0034-4257(00)00150-4.

[74] P. S. Thenkabail, R. B. Smith, and E. De Pauw, "Hyperspectral vegetation indices and their relationships with agricultural crop characteristics," *Remote Sens. Environ.*, vol. 71, no. 2, pp. 158–182, Feb. 2000, doi: 10.1016/S0034-4257(99)00067-X.

[75] Q. Zhang, T. Yao, K. F. Huemmrich, E. M. Middleton, A. Lyapustin, and Y. Wang, "Evaluating impacts of snow, surface water, soil and vegetation on empirical vegetation and snow indices for the Utqiaġvik tundra ecosystem in Alaska with the LVS3 model," *Remote Sens. Environ.*, vol. 240, Apr. 2020, Art. no. 111677, doi: 10.1016/j.rse.2020.111677.

[76] R. Wang, K. R. Springer, and J. A. Gamon, "Confounding effects of snow cover on remotely sensed vegetation indices of evergreen and deciduous trees: An experimental study," *Glob. Change Biol.*, vol. 29, no. 21, pp. 6120–6138, Nov. 2023, doi: 10.1111/gcb.16916.

[77] S. Roessler, A. Dietz, and S. Holzwarth, "A European time series of daily snow cover from AVHRR data over 36 years: Results of the timeline project," in *Proc. IEEE Int. Geosci. Remote Sens. Symp.*, Jul. 2023, pp. 114–117, doi: 10.1109/IGARSS52108.2023.10282415.

[78] S. Roessler and A. J. Dietz, "Development of global snow cover—Trends from 23 years of global snowpack," *Earth*, vol. 4, no. 1, pp. 1–22, 2023, doi: 10.3390/earth4010001.

[79] S. Rößler and A. J. Dietz, "Detection of snow cover from historical and recent AVHHR data—A thematic TIMELINE processor," *Geomatics*, vol. 2, no. 1, pp. 144–160, 2022, doi: 10.3390/geomatics2010009.

[80] L. Wang, F. Tian, Y. Wang, Z. Wu, G. Schurgers, and R. Fensholt, "Acceleration of global vegetation greenup from combined effects of climate change and human land management," *Glob. Change Biol.*, vol. 24, no. 11, pp. 5484–5499, Nov. 2018, doi: 10.1111/gcb.14369.

[81] S. I. Higgins, T. Conradi, and E. Muhoko, "Shifts in vegetation activity of terrestrial ecosystems attributable to climate trends," *Nature Geosci.*, vol. 16, no. 2, pp. 147–153, 2023, doi: 10.1038/s41561-022-01114-x.

[82] L. Zhao, A. Dai, and B. Dong, "Changes in global vegetation activity and its driving factors during 1982–2013," *Agricultural Forest Meteorol.*, vol. 249, pp. 198–209, 2018, doi: 10.1016/j.agrformet.2017.11.013.

[83] C. Grossiord et al., "Plant responses to rising vapor pressure deficit," *New Phytologist*, vol. 226, no. 6, pp. 1550–1566, Jun. 2020, doi: 10.1111/nph.16485.

[84] D. Chu et al., "Long time-series NDVI reconstruction in cloud-prone regions via spatio-temporal tensor completion," *Remote Sens. Environ.*, vol. 264, Oct. 2021, Art. no. 112632, doi: 10.1016/j.rse.2021.112632.

[85] M. Rhif, A. Ben Abbes, B. Martinez, R. de Jong, Y. F. Sang, and I. R. Farah, "Detection of trend and seasonal changes in non-stationary remote sensing data: Case study of Tunisia vegetation dynamics," *Ecol. Inform.*, vol. 69, Jul. 2022, Art. no. 101596, doi: 10.1016/j.ecoinf.2022.101596.

[86] X. Guan et al., "Fusing MODIS and AVHRR products to generate a global 1-km continuous NDVI time series covering four decades," *Big Earth Data*, vol. 9, no. 1, pp. 72–99, Jan. 2025, doi: 10.1080/20964471.2024.2448072.

Christina Eisfelder received the Dipl.-Ing. degree and the Ph.D. (Dr.-Ing.) degree in cartography from the Technical University of Dresden, Dresden, Germany, in 2008 and 2013, respectively.

Her diploma thesis dealt with object-based forest-type mapping based on very high resolution optical remote sensing data. Her dissertation was on modeling net primary productivity and above-ground biomass for mapping of spatial biomass distribution in Kazakhstan. Since 2008, she has been with the German Remote Sensing Data Center (DFD), German Aerospace Center (DLR), Oberpfaffenhofen, Germany. As a Research Scientist within the Department "Land Surface Dynamics," she has been involved in several international research projects. Her current research interests include remote sensing analyses in the context of vegetation dynamics and land surface monitoring, land cover and crop type mapping, phenological analyses, long time-series and trend analyses, and drought monitoring and early warning.

Soner Üreyen received the M.Sc. degree in geoinformatics from the Friedrich Schiller University of Jena (FSU), Jena, Germany, in 2015 and the Ph.D. degree in geography from the Julius Maximilians University of Wuerzburg (JMU), Wuerzburg, Germany, in 2022.

From 2018 to 2024, he was a doctoral student and a Postdoctoral Researcher with the German Aerospace Center, Oberpfaffenhofen, Germany. He is currently a Patent Examiner with the European Patent Office, Munich, Germany. His research interests include remote sensing time series, spatio-temporal analysis, and machine learning.

Sarah Asam received the M.Sc. degree in global change ecology from the University of Bayreuth, Bayreuth, Germany, in 2010 and the Ph.D. (Dr. rer. Nat.) degree in geography from the University of Würzburg, Würzburg, Germany, in 2015.

Her dissertation was on the potential of high-resolution remote sensing data for leaf area index derivation using statistical and physical models. From 2014 to 2017, she was a Postdoc Scientist with the Institute for Earth Observation, Eurac Research, Bolzano, Italy. From 2017 to 2020, she was a Project Manager of the TIMe Series Processing of Medium Resolution Earth Observation Data assessing Long-Term Dynamics In our Natural Environment (TIMELINE) project, facilitating the analysis of multidecadal AVHRR time series. Since 2017, she has been a Research Scientist with the Agricultural and Forest Ecosystems Team, Department of Land Surface Dynamics, German Remote Sensing Data Center, Oberpfaffenhofen, Germany. Her research interests include the mapping and characterization of vegetation in agricultural, grassland, and forest ecosystems, using time series, cover fraction analysis, and classification approaches.

Andreas Hirner received M.Sc. degree in geology from the Ludwig-Maximilians-University Munich, Munich, Germany, in 1996 and the Ph.D. degree in geology from the University of the Witwatersrand, Johannesburg, South Africa, in 2002.

After working as a Spatial Software Developer for a small startup, he began his first stint with the German Remote Sensing Data Center (DFD), German Aerospace Center (DLR) in 2003, where he worked for six years as a Research Scientist in the Sino-German coal fire project. From 2009 to 2012, he had a contract with the Critech unit, Joint Research Center (JRC) of the European Commission, Ispra, Italy, where he was involved in crisis management in response to natural disasters. After that, he returned to DFD/DLR, Wessling, Germany. Since the last more than ten years, he has been a Research Scientist with the Department "Land Surface Dynamics" on various projects. His focus currently is on vegetation dynamics and large-scale processing of geospatial data using the latest developments in machine learning.

Philipp Reiners received the Master of Science degree in physical geography from the University of Marburg, Marburg, Germany, in 2019. Since 2022, he has been working toward the Ph.D. degree in geography with the Land Surface Department, German Aerospace Center, German Remote Sensing Data Center, Wessling, Germany.

Since 2019, he has been a Research Scientist with the Land Surface Department, German Aerospace Center, German Remote Sensing Data Center, Wessling. During his Ph.D., he developed a long-term data record of 40 years of land and sea surface temperature from AVHRR data over Europe and North Africa. His special research interests include thermal remote sensing, climatology, time series analysis, calibration, and validation.

Juliane Huth received the Dipl.-Ing. degree in geodesy from the Karlsruhe Institute of Technology, Karlsruhe, Germany, in 2004.

Since 2007, she has been working with the German Remote Sensing Data Center of the German Aerospace Center (DLR), Wessling, Germany. She is currently leading a group for remote sensing applications for coasts and river basins. Her research interests include the effects of climate change and extreme climatic events on natural ecosystems and the human-influenced environment in general.

Felix Bachofer received the Ph.D. degree in geography in 2016 from the University of Tuebingen, Tuebingen, Germany.

Since 2020, he has been the Head of the "Coasts and River Basins" Research Team with the Earth Observation Center, German Aerospace Center (DLR), Wessling, Germany. He has been subsequently involved as a Postdoctoral Researcher in various environmental and geospatial research projects. In 2018, he became a Researcher with DLR, where he has been actively involved in managing several research projects. His research pursuits primarily revolve around the exploration of urban development, coastal areas, flood and drought dynamics, and the intricate relationships between these factors and climate change, all through the lens of multisensor remote sensing.

Martin Bachmann received the Dipl.-Geogr. degree in geography from the Technical University of Dresden, Dresden, Germany, in 2002, and the Ph.D. (Dr. rer. nat.) degree in geography from the University of Würzburg, Würzburg, Germany, in 2007.

Since 2005, he has been a Research Scientist with the Land Applications Department, German Remote Sensing Data Center, German Aerospace Center (DLR), Wessling, Germany, leading the team "Applied Spectroscopy" between 2009 and 2013. He leads the work package on "Data Quality Control" within the EnMAP ground segment and within the DESIS ground segment, including vicarious calibration and validation activities for these imaging spectrometers. For the upcoming ESA CHIME mission, he is leading the L2B thematic processor part. His research interests also include the application of field and imaging spectroscopy for land degradation applications.

He is currently active within the CEOS WGCV IVOS on Infrared and Visible Optical Sensors, within CEOS LSI-VC activities toward Analysis Ready Data, cochairing the EARSeL SIG-IS, being Secretary of the ISPRS WG I/3 (Multispectral, Hyperspectral and Thermal Sensors), and a member of the Mission Advisory Group of the ESA "TRUTHS" spectrometer mission.

Stefanie Holzwarth received the engineering degree in geodesy from the University of Stuttgart, Stuttgart, Germany, in 2002.

Since 2002, she has been a Research Scientist with the Department of Land Surface Dynamics, German Remote Sensing Data Center, Oberpfaffenhofen, Germany. She has more than 20 years of experience in hyperspectral remote sensing. Since 2020, she has been a Project Manager of the TIMELINE project (TIMe Series Processing of Medium Resolution Earth Observation Data Assessing Long-Term Dynamics in Our Natural Environment). Her research interests include the application of remote sensing for forest monitoring.

Claudia Kuenzer received the diploma (M.Sc.) degree in geography from the University of Trier, Trier, Germany, in 2001 and the Ph.D. degree in remote sensing from the TU Vienna, Vienna, Austria, in 2005.

From 2001 to 2006, she was a Research Associate with the German Remote Sensing Data Center, German Aerospace Center, Germany. In 2005, she spent half a year as a Guest Scientist with the Institute of Remote Sensing Applications, and Beijing Normal University, Beijing, China. From 2006 to 2008, she held a position as a Postdoc Scientist and an Institute Assistant with the Institute of Photogrammetry and Remote Sensing, TU Vienna. Since 2008, she has been back with the Earth Observation Center, where she acted as a Research Group Leader and a Science Coordinator of several large interdisciplinary international projects. Since 2016, she has been the Head of the Department "Land Surface Dynamics" with the Earth Observation Center, German Aerospace Center, Oberpfaffenhofen, Germany. She is currently a Professor of remote sensing and geosciences. She currently supervises 12 Ph.D. students and two habilitation candidates. She has contributed to more than 180 SCI journal papers and more than 200 conference proceedings. Her research interests include remote sensing applications for the assessment of land surface dynamics based on long time series analyses and deep learning.